ANALYTICAL AND NUMERICAL STUDIES OF HEAT AND MOISTURE TRANSFER THROUGH POROUS INSULATION

By

BI-FENG ZHENG

B. Sc. (Thermal Science and Engineering) Zhejiang University , China

M. Sc. (Thermal Science and Engineering) Zhejiang University, China

A THESIS SUBMITTED IN PARTIAL FULFILLMENT OF

THE REQUIREMENTS FOR THE DEGREE OF

MASTER OF APPLIED SCIENCE

in

THE FACULTY OF GRADUATE STUDIES

DEPARTMENT OF MECHANICAL ENGINEERING

We accept this thesis as conforming

to the required standard

In presenting this thesis in partial fulfilment of the requirements for an advanced degree at the University of British Columbia, I agree that the Library shall make it freely available for reference and study. I further agree that permission for extensive copying of this thesis for scholarly purposes may be granted by the head of my department or by his or her representatives. It is understood that copying or publication of this thesis for financial gain shall not be allowed without my written permission.

Department of Mechanical Engineering

The University of British Columbia

2324 Main Mall

Vancouver, Canada

V6T 1Z4

Date: October 14, 1993

Abstract

This work contains both analytical and numerical studies of heat and moisture transport through a porous insulation in the presence of condensation, with impermeable, adiabatic vertical boundaries, and with one horizontal boundary facing a warm humid ambient and the other facing a cold impermeable surface.

The analytical model is developed for heat and water vapor transfer in flat-slab and round-pipe thermal insulations. The model is validated by comparing its predictions with available experimental data. The effective thermal conductivity of the insulation in the presence of condensation depends on seven design and operating variables. The effect of these variables is determined by a parametric study. For practical operating conditions, the effective thermal conductivity varies from about 1.5 to 15 times the dry-state value. The computed data are presented in the form of design curves which may be used to estimate the effective thermal conductivity for flat-slab and round-pipe insulation systems.

The analysis in this work quantifies the process of energy and mass transport in a porous insulation. A rigorous and fundamental formulation of heat and mass transfer in the insulation system is presented. The problem is modeled as one-dimensional, transient, multiphase flow with variable properties. Four stages in the energy and moisture transport process are identified, and they are formulated by a system of transient inter-coupled equations and several thermodynamic relations using a local volume averaging technique. The numerical results are compared with experimental data for five different operating conditions and for times up to 600 hours. The model predicts the temperature distribution, heat transfer rate, the total moisture gain successfully. The predicted

liquid distributions agree well with measured data for a period of up to 70 hours. The interesting effects of pertinent parameters on the energy and moisture transfer in the porous insulation are investigated. The present study, which for the first time presents a full simulation of the problem considering the mobile condensate, can be applied to other classes of problems on heat and mass transfer with phase change through a porous medium.

Table of Contents

List of Tables

List of Figures

Nomenclature

a	constant in Clausius-Clapeyron relation, Eq. (4.26)
a	coefficient in linear discretized equations
b	constant in Clausius-Clapeyron relation, Eq. (4.26)
b_1	constant in Equation (4.16)
b_2	constant in Equation (4.16)
B	Biot number, $h^* L / k^*_{eff}$
B_m	mass transfer Biot number, $h^*_m L / D^*_{v,eff}$
c_p	dimensionless heat capacity at constant pressure
C(z)	dimensionless concentration of vapour
C_a	dimensionless concentration of vapour in ambient
C_c	dimensionless concentration of vapour at dry-wet interface
D_v	dimensionless vapor diffusion coefficient
D_l	dimensionless liquid diffusion coefficient defined in Eq. (6.26)
D_β	dimensionless liquid diffusion coefficient defined in Eq. (3.4)
D_{12}	binary diffusion coefficient of Fick's law [m/s^2]
$f(\theta)$	dimensionless function for concentration
$f'(\theta)$	df/dθ
Fo	Fourier number, $\dfrac{t^*}{L^2/\alpha^*_{0,eff}}$
g(T)	Clausius - Clapeyron relation [kg/kg(dry air)]
G	dimensionless condensation rate defined in analytical study
G^*	dimensionless condensation rate defined in numerical study
h	dimensionless heat transfer coefficient in ambient

h_{fg}	enthalpy of vaporization [kJ/kg]
h_m	dimensionless mass transfer coefficient in ambient
k	dimensionless thermal conductivity
k_{dry}	dry thermal conductivity [W/m K]
k_{eff}	effective thermal conductivity defined in Eq. (4.29) [W/m K]
k_{eq}	equivalent thermal conductivity defined in Eq. (7.1) [W/m K]
K(w)	hydaulic conductivity
L	length of slab [m]
L_e	Lewis number, α^*/D_v^*
L_{eq}	equivalent slab length [m]
m(x)	vapor concentration [kg/kg (dry air)]
m_a	vapor concentration in ambient [kg/kg (dry air)]
m_2	saturation concentration at temperature T_2 [kg/kg(dry air)]
p_a	dimensionless partial pressure of air
p_{total}	dimensionless total pressure of gas phases
p_v	dimensionless partial pressure of vapor
$P_1 - P_5$	dimensionless parameters defined in Eq. (6.10)
R_a	air gas constant [N m/kg K]
R_v	vapor gas constant [N m/kg K]
q	dimensionless heat flux at cold surface
$\overline{q}$	heat flux at cold surface [W/m^2]
Q	dimensionless heat flux
Q'	dimensionless heat flux in Reference [38]
r	radius of pipe insulation [m]
r_o	outer radius of pipe insulation [m]

r_i	inner radius of pipe insulation [m]
T(x)	temperature distribution [K]
T_0	reference temperature in Clausius-Clapeyron relation [K]
T_a	ambient temperature [K]
T_2	temperature of cold surface [K]
S	liquid saturation
V	volume of porous insulation [m³]
V_m	main stream velocity [m/s]
w	weight liquid content
x	distance along slab [m]
y	transformed variable [m]
z	dimensionless distance
z_d	dimensionless dry length
$\alpha^*_{0,eff}$	effective thermal diffusivity, $k_0^*/\rho_0^* c_{p,0}^*$
β	dimensionless group
ϵ	volumetric fraction
ϵ_0	porosity (void fraction)
$\overline{\Phi}$	vapour flux [kg/m² s]
Φ	dimensionless vapour flux
ρ_a	density of air [kg/m³]
Γ	condensation rate per unit volume [kg/m³ s]
τ	tortuosity factor
$\theta(z)$	dimensionless temperature distribution
θ_c	dimensionless temperature at the dry-wet interface

Subscripts

0	initial value
2	value at cold surface
a	ambient
a	air phase
d	dry
e	east side control volume face
eff	effective
E	east side grid point
i	i-th phase
P	central grid point
ref	reference
v	vapor phase
w	west east side control volume face
W	west side grid point
β	liquid phase
γ	gas phase
σ	solid phase

Superscripts

*	dimensional value
0	value in previous time step

Acknowledgement

I wish to express sincere gratitude to Dr. M. Iqbal and Dr. E. G. Hauptmann for their supervision and continuous encouragement through all stages of this work. Financial assistance from the National Science and Engineering Research Council of Canada is gratefully appreciated.

My thanks go to Dr. Wijeysundera from The National University of Singapore who generously offered the experimental data. His valuable suggestions, comments, and discussions during his sabbatical leave at the Department of Mechanical Engineering, UBC were also very helpful.

This thesis is dedicated to my wife, Wei-Hung, her understanding and support made the completion of this work possible.

Chapter 1

INTRODUCTION

1.1 Background

Heat and mass transfer in porous media accompanied by phase change is a phenomenon which occurs frequently in nature and in many engineering applications. These applications are in the area of chemical , environmental, mechanical and petroleum engineering, geology and others. In recent years, heat and moisture transfer through fibrous insulation has drawn considerable attention among many investigators because of applications in the energy management of buildings, and heated and refrigerated building envelopes.

Fibrous insulation is used within building sections, such as partition walls, ceilings, roofs, floors etc, to separate the heated space from the unheated space. In air conditioning systems, fibrous insulation is commonly used to insulate the chilled water pipes and cold air ducts. In these applications, vapor barriers are applied to prevent water vapor ingress from the ambient. However, because of factors such as poor installation, cracks develop with age, particularly near joints, clamps and supports. The water vapor will migrate into the insulation. Water vapor condensation can take place anywhere in a porous insulation when the vapor density is greater than the saturation vapor density which corresponds to the local temperature at that point. The condensation effect is especially prominent when the insulating material is exposed to large temperature differences and high humidity environments. As condensation occurs, the liquid phase resulting from condensation will cause a significant increase in heat transfer across the insulation and

hence it affects the thermal performance of the insulation. The long term effects of condensation are corrosion of the metallic components of the insulated system and the eventual destruction of insulation.

1.2 Physical Process Description

The heat and moisture transfer in porous insulation is generally a complex multidimensional problem including vapor transport by diffusion and convection, flow of liquid due to gravity and capillary action, and condensation or freezing accompanied by release or consumption of latent heat. The solution of this entire problem is not attempted here. Instead, the problem is reduced to a one-dimensional configuration which still retains most of the important parameters of the original problem.

The one-dimensional configuration investigated here is shown in Figure 1.1 An initial dry fibrous insulation has two boundaries which encounter two different environments: one of the boundary faces a cold, impermeable plate with temperature T_2, the other boundary is exposed to a warm humid ambient air, with temperature T_a, humidity RH, vapor concentration C_a, convective heat transfer coefficient h_a, and mass transfer coefficient h_m.

The water vapor will migrate into the insulation slab due to the vapor concentration gradient and the thermal gradient, and it is expected to exhibit four stages of transport processes as shown in Figure 1.2.

The first stage is a relatively short initial transient stage in which the temperature and vapor concentration fields are developing within the insulation slab. During this process, a very small quantity of liquid water accumulates in the porous medium. Condensation is defined here as the accumulation of liquid beyond the adsorption process in which the vapor reaches the saturation concentration at a given temperature. The region in which
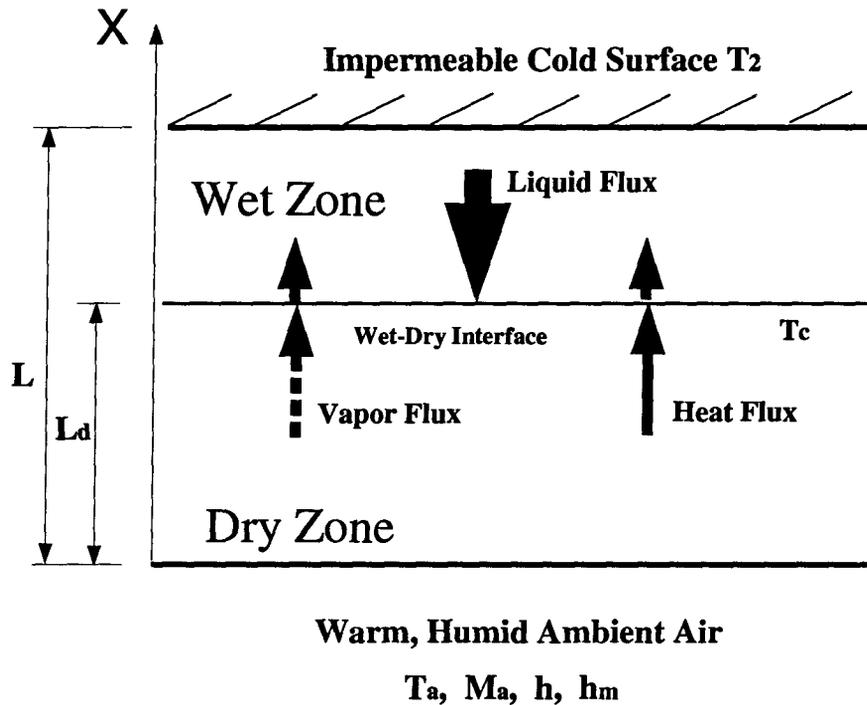
Figure 1.1: Schematic Diagram of Physical Problem.

the air-vapor mixture is saturated is referred to as the wet region where condensation takes place. The wet region is established , and the wet and dry region is separated by the wet-dry interface after this stage.

In the second stage, the heat and vapor transfer processes reach a quasi-steady state, and the temperature and vapor concentration fields are invariable with time. Liquid is accumulated in the wet region, however the amount of liquid content is still low and does not have a significant effect on transport properties.

When liquid accumulation exceeds a value high enough as to affect the properties significantly, the liquid starts to move due to generated liquid pressure and will flow towards the wet-dry interface and towards the drier, warmer surface by capillary action. The wet-dry interface is moving as the wet region expands due to the liquid outflow.

In the last stage, the wet-dry interface eventually reaches the exposed surface, The

T2 ///////////////

Condensate

Dry Insulation

Ta ↑↑↑↑↑↑↑↑
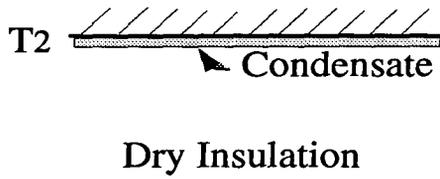
(a) Initial Stage: Condensation
at Cold Plate.

T2 ///////////////

Wet Region

Wet-dry Interface

Ta ↑↑↑↑↑↑↑↑↑
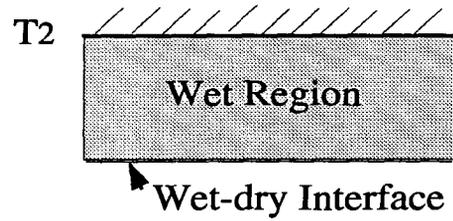
(b) Quasi-steady Stage:
Liquid Accumulation in
the Wet Region.

T2 ///////////////

Wet Region

Dry Region

Ta ↑↑↑↑↑↑↑↑
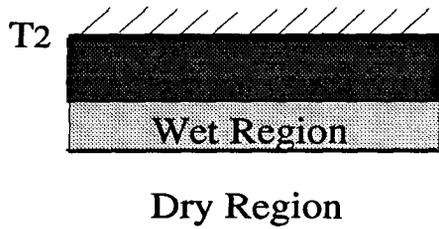
(c) Liquid Diffusion Stage:
Liquid Diffusion Starting
from Cold Surface.

T2 ///////////////

Ta ↑↑↑↑↑↑↑↑
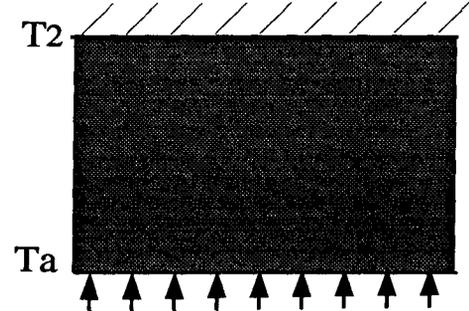
(d) Long Term Stage:
Liquid Accumulation and
Diffusion in Entire Slab.

Dry Region

Liquid Diffusion Region

Wet Region
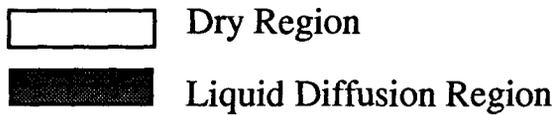
Figure 1.2: Four Stages in Energy and Moisture Transport Process.

effects of liquid accumulation and liquid flow become dominant. The accumulation of liquid in the insulation is believed to have two important effects: (1). decrease in the local vapor diffusion coefficient, (2) increase in local thermal conductivity of the slab. These factors will both influence the heat transfer and condensation rate in the slab.

1.3 Geometrical Characteristic of Fibrous Insulation

The Fiberglass batts used as thermal insulation consist of layers of Fiberglass filaments that are held together with a phenolic binder. The batts usually have a very high void fraction (95-99 percent). The Fiberglass filaments have varying diameters with an average value of $3.56(10)^{-6}$ m. Each Fiberglass layer differs from its adjacent layers and has a different void fraction. The Fiberglass filaments are dispersed randomly in each layer. However, the number of fibers along the batt is slightly larger than that across the batt, and the number of fibers that are perpendicular to the batt and run from one layer to the other is very small.

Generally speaking, fibrous insulation is an inhomogeneous assemblage of Fiberglass filaments and phenolic binder. The insulation is characterized by an anisotropic fiber density and a nonuniform void fraction.

1.4 Motivation of the Present Study

A detailed study for the entire transport process in fibrous insulation is complicated by the following factors:

- Heat and mass transport in porous insulation is a problem with multiphase flow. In general a wet porous insulation consists of three phases: the solid matrix, the liquid water, and a binary gas phase composed of air and water vapor.

- The transport mechanisms involved in the process are quite complicated. Energy transport in such a medium occurs by conduction in all of the phases as well as by convection with those phases which are able to move. In addition, there is heat transfer caused by phase change at the interface between liquid and gas. Mass transfer occurs within the voids of the medium. In an unsaturated state, these voids are partially filled with a liquid, whereas the rest of the voids contains air and water vapor. In the gas phase, there is vapor diffusion due to the vapor concentration gradients, bulk convection due to the density variation induced by temperature gradients, and air infiltration due to the small difference in gas pressure across the insulation. The flow of liquid is caused by internal forces, such as capillary, intermolecular and osmotic forces, and external forces, such as imposed pressure difference, and gravity.

- The transport properties involved vary strongly with structure of the porous medium, moisture content and temperature.

- It is almost impossible to study quantitatively the transport processes for the irregular void configurations which exist in general in porous insulation. It is still difficult even for a regularly shaped matrix.

Thus there is indeed a need for a rigorous and extensive investigation of the heat and mass transport processes in porous insulation. This may lead to better estimation of insulation properties for building design purposes.

In the present work, the focus is on the analysis of the process of moisture accumulation and transport in the fore-mentioned insulation system, and as well as the effect of moisture on thermal performance of insulation. The entire process of energy and mass transport in the porous insulation system is quantified and the significant transport mechanisms are identified. A simplified formulation for four stages of the transport process is

presented to simulate the transient and spatial variation of the pertinent variables. An analytical model is also presented to perform a parametric study on the thermal performance of porous insulation in the presence of condensation. Both the analytical and transient numerical model are validated by comparing with experimental data. Finally the interesting effects of variation of pertinent parameters on the energy and moisture transfer are investigated.

Chapter 2

A BRIEF REVIEW OF LITERATURE

2.1 Background

The importance of heat and mass transport in a porous medium is well appreciated. The early treatments of liquid flow and heat transfer in a porous medium were more empirical rather than rigorously theoretical. The initial macroscopic treatments on water flow through a porous medium were made in the 1880's [2]. The porous medium, which is a heterogeneous system made of a solid matrix with its void filled with gases and liquids, can be treated as a continuum by properly accounting for the role of transport through each phase in this system of phases. The attempt at microscopic (pore-level) transport studies began in the early 1900's [2]. The pore-level analysis offered a better understanding of heat and mass transport, however the description and solution of a transport problem at the microscopic level is impractical and, perhaps impossible because the geometry of the surface that bounds the phase is not observable and is too complex to be described. The macroscopic level approach, at which continuous and differentiable quantities may be determined, is needed to model and predict the heat and mass transport in a porous medium. Progress was achieved in the second half of this century with the more rigorous approaches of local volume averaging techniques [3].

Early studies on transport in porous insulation were mainly on the motion of liquid through unsaturated porous media. In early papers, heat transfer was not given sufficient attention until Krischer (1940) [4]. Probably one of the most significant contributors to

heat and mass transfer in porous media, Krischer first considered seriously the intimate role that transport of energy may play in moisture transfer in a porous medium. Prior to Philip and DeVries (1957) [5], moisture movement was explained by a simple diffusion theory, the flux being given by Fick's law. Philip and DeVries (1957) [5] and DeVries (1958) [6] extented the theory and generalized the effects of capillary flow, vapor transport and energy transfer, and represented the transport due to capillary forces in terms of gradients of moisture content and temperature. Their work consolidated most of the previous knowledge on the influence of temperature gradients on moisture movement and laid the groundwork for a better understanding of simultaneous heat and water movement in soil.

Extensive research on heat and mass transfer in porous media has been done by the Soviet scientist, Luikov (1966, 1975)[7, 8]. He described heat and mass transfer as caused both by the temperature and the liquid concentration gradient, and developed a mechanistic approach for the representation of simultaneous heat and moisture transfer in dying processes. A set of linear mass and heat transport equations were derived. However, the effect of phase change was not considered and the dependence of transport coefficients on temperature and concentration were neglected.

Whitaker (1977) [3] presented general formulations of simultaneous heat, mass and momentum transfer in porous media. The intrinsic phase averaged quantities were defined at the appropriate level and the continuum point equations which are averaged were described.

Although simultaneous heat and moisture transfer in a porous medium has been studied by many other researchers [9, 10, 11], most of the work has been directed towards studies of soils and sands. Very little attention has been given to fibrous insulating materials until the last fifteen years.

2.2 Experimental Studies

The experimental investigation of porous insulation has focused mainly on two aspects: 1). the effect of moisture gain by porous insulation on thermal conductivity of and heat transfer through the insulation; 2). transport of liquid condensate within insulation.

Jespersen (1953) [12] measured the thermal conductivity of a 62 kg/m³ glass fiber, using a steady heat flow method, but with a very small gradient of temperature across the sample in order to get a uniform moisture distribution. Joy (1957) [13] worked on 96 kg/m³ fibrous insulation, using a transient heat flow method. Their results show a significant increase of thermal conductivity even for a very low moisture contents.

Similar measurements to Jespersen and Joy's work have been performed by Langlais (1982) [14], using a classic steady-state method. The thermal conductivity of a high density mineral fiberboard was determined as a function of moisture content. However, their results show that thermal conductivity is far less affected for low moisture content. They explained that their differences with Joy's results are due to the non-uniform moisture distribution under the influence of the temperature gradient. Bomberg and Shirtliffe (1978)[15] also demonstrated the influence of this redistribution on thermal conductivity. The moisture redistribution process was also studied experimentally by Kumaran (1987, 1988) [16, 17] in an insulation slab under the influence of a temperature gradient.

Langlas et al. (1983) [18] and Langlais and Klarsfeld (1984) [19] further studied the effects of moisture transfer through an insulation slab under two sets of boundary conditions and pointed out that the rapid variations in thermal conductivity values were due to moisture phase change and diffusion. Thomas et al. (1983) [20] measured the moisture and temperature distribution , as well as the thermal conductivity versus time. Modi and Benner (1985, 1986)[21, 22] measured the moisture gain of spray-applied fiber-glass and cellulose insulation slabs from the surroundings and also the effect of the moisture

gain on the thermal conductivity.

Wijeysundera et al. (1989) [23, 24] conducted two series of experiments to study the diffusion and condensation of water vapor in fiber-glass. The first set of experiments were tests on fibrous insulation. In the second series of experiments, one of the faces of the insulation slab was exposed to a warm and humid ambient and the other one was maintained at a low temperature. The temperature and liquid distribution, the total moisture gain, the heat flux were measured for a range of experimental conditions. Further experimental studies on effects of moisture gain by a fiber glass insulation slab in a second set experimental conditions were reported by Wijeysundera (1992) [25]. The major heat and moisture transfer parameters were measured over a period of up to 600 hours.

The transport of the liquid condensate within fibrous insulation has received less attention. Motakef and El-Masri (1985) [26] presented a model for the isothermal liquid diffusion in fibrous insulation in the absence of gravitational forces. The model related the liquid diffusion to the characteristics of the insulation, such as void fraction, spatial distribution, directionally index, tortuousity factor etc. Experimental data was also reported to verify the model. Timusk and Tenende (1988) [27] studied the capillary rise of water in fiber glass slabs. Cid and Crausse (1990) [28] measured the coefficient of liquid diffusion which was correlated to moisture content and the nominal density of the solid phase, based on the principle of attenuation of two radioactive emissions. Although the thermal effects were not added to the measurements, so doing would makes it possible to predict the behavior of the materials when they are submitted to moisture.

Extensive field studies of heat transfer through wet insulation have been reported by Heldlin (1988) [29], during all seasons of the year.

2.3 Theoretical Studies

As mentioned in the beginning of this Chapter, simultaneous heat and mass transfer has been extensively studied for various systems [3-11]. However, these studies have been only recently extended to heat and moisture transfer in insulation . Dinulescu and Eckert (1980) [30] analyzed the moisture migration in a slab of an unsaturated porous medium between two impermeable surfaces.

The problem of condensation in insulation was first studied by Ogniewicz and Tien (1980) [31]. The condensation process in insulation is characterized in terms of three regimes, and a quasi-steady model was presented to studied the condensation effects in the second regime, where coupling between temperature and concentration of the condensing vapor was taken into account.

Motakef and El-Masri (1986) [32] presented a one-dimensional analytical model for heat and mass transport with phase change in a porous slab similar to Oganiewcz and Tien [31], and the closed-form approximate solutions for two limiting regimes of condensate diffusivity were reported. The same problem was also modeled by Vafai and Sarkar(1986) [33] as a transient, multiphase flow, with variable properties. The formulation was based on the local volume-averaging technique for each phase to come up with the governing equations for the condensation process in fibrous insulation. However, the simplifying assumption that liquid accumulation is small was made in arriving at the solution.

Shapiro and Motekef (1989) [34] extended their analysis to unsteady transport processes and reduced the unsteady process to that of quasi-steady fields in time-dependent domains corresponding to mobile and immobile condensates. The model underpredicts the energy transfer in the wet zone and the range of validity of the solutions is limited , especially for the mobile condensate.

Vafai and Whitaker (1986) [35] first reported a two-dimensional unsteady numerical work with simplifying assumptions. Vafai and Tien (1988, 1989) [36, 37] performed a more thorough numerical simulation of the two-dimensional multiphase transport process in a porous medium. Information was presented on the variation and the intercoupling effects of the important field variables, the effects of some parameters such as humidity levels, the porosity etc. on the condensation rate, liquid accumulation and energy transfer. However, No attempt was made to verify numerical solutions by comparison with experimental data. The computational results presented in the paper only show the transport process within the first 500 seconds. In such a short initial period, the absorption process of bounded liquid is still in the initial stage, the effects of temperature gradient and condensation are not significant, and the contribution to the heat and mass transfer in insulation is small considering the long term impact of accumulation and transport of the liquid condensate through the insulation. In addition to, the treatment used in their scheme to determine when condensation should be taken into account lacks either experimental validity or theoretical support.

Wijeysundera et al. [23, 25] used a semi-empirical model to interpret some of their experimental results. The analytical model developed for transport process during the quasi-steady phase has given good predictions of heat and vapor flow through insulation for low level of moisture transfer.

Tao et al. (1991) [38] analyzed the moisture and frost accumulation in a glass-fiber slab. An approach similar to the study of Vafai and Sarker [32], who used the local volume average technique, was applied to the case with temperature below the triple point of water. A numerical simulation was performed for one-dimensional, transient, vapor diffusion with phase changes and variable properties.

2.4 Scope and Objectives of the Present Study

It is clear from the literature survey that the transfer processes in insulation can be quantified by a). field and laboratory studies, b). analytical/numerical studies. Generally speaking, the field and laboratory studies are time consuming due to the slow process of moisture transfer. Furthermore, it is difficult to cover the effects of such a wide range of operating and design parameters.

The available analytical studies mainly dealt with the quasi-steady phase of the transfer processes. Although several investigators have reported good predictions with their models, the performance of insulation in the presence of condensation has not been sufficiently analyzed. From a design stand-point, it is important to study the effects of moisture on thermal performance of insulation under practical operating conditions.

Less work has been done to simulate numerically the full transport processes which the insulation may undergo for a long time period in the presence of condensation. The long term effects of condensation on the performance of insulation has not been studied theoretically.

The present study focus on the analytical and numerical investigation of the transfer processes through fibrous insulation in the presence of condensation. The objectives of this study are :

1). To perform a detailed and parametric study on effects of condensation on the thermal performance of insulation in the quasi-steady phase. The analytical models based on the quasi-steady models by Wijeysundera et al. [22] will be extended to cover the main design and operating parameters on which the effective thermal conductivity depends, with the hope that the modified model will be able to to predict the most important heat and mass transfer performance for engineering design and application purposes.

2). To perform a numerical simulation study that covers all the phases mentioned in Chapter one, and also uses measured physical property variations available in the literature. The numerical results will be compared with the experimental data by Wijey-sundera et al. [22,23]. Accordingly, the analytical and numerical models will be derived, and the computer codes developed.

Chapter 3

MATHEMATICAL DESCRIPTION

3.1 Introduction

This chapter presents the background for the general mathematical models that describe transport of heat and mass in porous insulation at a macroscopic level. The general formulation of this problem is based on the local volume-averaging technique [3] for mass, momentum, and energy equations for each phase which make up the governing equations for heat and mass transport process in insulation. The general governing equations for the transport of energy, water vapor and liquid, together with constitutive relations are described. The limitations and restrictions of the governing equations are stated and the validity of the assumptions are discussed.

3.2 Continuum Approach

Porous insulation is a multiphase system, where the various phases are separated from each other by an abrupt interface. It is difficult to formulate the transport problem including the interface boundaries between each phase. The conventional treatment is to replace the real system, where the multiphases together occupy disjoint subdomains within a porous medium, with a model in which each phase is assumed to behave as a continuum over the whole domain.

With the continuum approach, the average values of phase variable are taken over elementary volumes, centered at the point. By assigning average values to every point,

the variables which are differentiable functions of the space coordinates can be obtained.

The continuum approach is thought reasonable since it circumvents the needs to specify the exact configuration of the interface boundaries, and it also is useful in solving field problems of practical interest due to its measurable quantities. The information regarding interface boundaries and the actual variation of quantities within each phase still remain in the form of coefficients. The numerical values of these coefficients must be determined experimentally for a specific porous media, in the laboratory, or in the field.

3.3 Local Volume Average Technique

The local volume technique is applied by associating with every point in the porous medium an averaging volume V that is bounded by a closed spatial surface A, as shown in Fig. 3.1. In general, the volume V is composed of three phases. These are: the solid phase V_σ, the liquid phase $V_\beta(t)$, and the gas phase $V_\gamma(t)$. At any location in space z, a quantity y is said to be spatially averaged when it is defined as

$$< y > (z) = \frac{1}{V(z)} \int_{V(z)} y dV. \tag{3.1}$$

A quantity in phase α is said to be intrinsic phase averaged when it is defined as

$$< y >_\alpha = \frac{1}{V_\alpha}(t) \int_{V_\alpha(t)} y_\alpha dV, \tag{3.2}$$

where y_α is zero in phases other than the α phase, and $< y >_\alpha$ is the mean value of y in V_α. In this study, the averaging symbols are omitted in order to simplify the notation.

The derivation of the general governing equations for heat and mass transfer in a porous insulation is based on Whitaker's work [3]. Several assumptions are made to arrive at the governing equations.
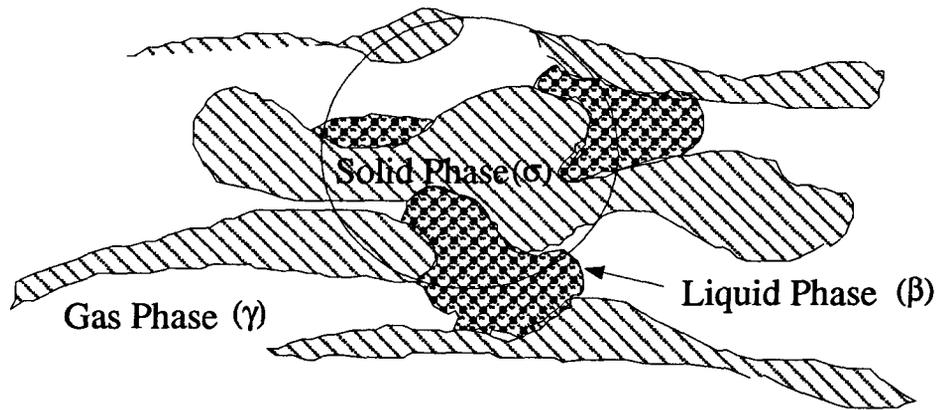
Figure 3.1: Macroscopic Average Volume Element.

3.4 Basic Assumptions

(1). The fibrous insulation is homogeneous and isotropic. This assumption is the common simplying procedure to rationally tackle the problems for heat and mass transfer in porous materials. The structure of the porous media is difficult to characterize. Motakef et al. [26] has been able to correlate diffusion of liquid using the void fraction, pore size distribution, tortuosity and so on. It seems clear that describing the parameters characterizing the structure will be a most difficult task for porous insulation, therefore the present theoretical development is restricted to the case where the structure parameters are independent of the spatial coordinates.

(2). The solid-liquid-gas system is in local thermal equilibrium. Since the heat and mass transport process investigated here, as well as most of drying processes, are characterized by no or relatively low convective transport rates, under these circumstances one could therefore assume that conductive transport is sufficient to eliminate significant temperature differences between the separated phases.

(3). No convective gas phase flow occurs in the insulation matrix; any moisture accumulation is caused by vapor diffusion only. In the present physical model, the effects of air infiltration are not included. This restriction might be removed in further studies.

(4). The total gas phase pressure in the insulation matrix is constant. This assumption is usually justified for drying process and building envelopes.

5). The gravitational effect on the liquid motion is negligible. Under the assumptions (3) and (4), the gas and liquid pressure distribution can be considered to be hydrostatic. Thus the forces exerted on the liquid phase are of two kinds: surface tension and gravity forces. For porous insulation with very small pores, the effect of gravity can be neglected due to the large surface tension forces. The experimental observation by Wijeysundera et al. [25] showed that after long term testing up to more than 300 hours, no liquid was observed to drip from a totally wet insulation slab.

3.5 Governing Equations

The derivation of governing equations requires considerable algebraic manipulation. As a result, they are taken directly from Whitaker's work [3]. The governing equations for water vapor, liquid, and energy transport are given as the following:

Vapor diffusion equation:

$$\frac{\partial}{\partial x}[D_v^*(T)\frac{\partial \rho_v^*}{\partial x}] - \Gamma = \frac{\partial(\epsilon_\gamma \rho_v^*)}{\partial t^*}.$$

(3.3)

Liquid transport equation:

$$\rho_\beta^* \frac{\partial}{\partial x}[D_\beta^*(w)\frac{\partial \epsilon_\beta}{\partial x}] + \Gamma = \rho_\beta^* \frac{\partial \epsilon_\beta}{\partial t^*}.$$

(3.4)

Energy equation:

$$\frac{\partial}{\partial x}[k^*(w)\frac{\partial T}{\partial x}] + h_{fg}\Gamma = \rho^* c_p^* \frac{\partial T}{\partial t^*}. \tag{3.5}$$

3.6   Constitutive Correlations

<u>Volumetric Constrain:</u>

The volume fractions for the three phases are defined as

$$\epsilon_\sigma = V_\sigma/V, \qquad \epsilon_\beta = V_\beta(t)/V, \qquad \epsilon_\gamma = V_\gamma/V(t). \tag{3.6}$$

Therefore the sum of these fraction is one,

$$\epsilon_\sigma + \epsilon_\beta + \epsilon_\gamma = 1. \tag{3.7}$$

<u>Thermodynamic Relations:</u>

Some thermodynamic relations are needed to connect the thermal energy equation with the vapor diffusion equation. By treating the gas phase as ideal gas, the air and vapor density can be determined by

$$p_a^* = R_a \rho_a^* T, \tag{3.8}$$

$$p_v^* = R_v \rho_a^* T. \tag{3.9}$$

The vapor pressure-temperature relation for the vaporizing gas can be represented by the Clausius-Clapeyron equation:

$$p_v^* = p_{v0}^* exp[\frac{h_{fg}}{R_v}(\frac{1}{T} - \frac{1}{T_{ref}})]. \tag{3.10}$$

The limitation of the Clausius-Clapeyron relation is that the gas-liquid interface is assumed flat, that is surface tension effects are not significant. When the effects of curvature and surface tension are important, the Kelvin equation may be used to represent the vapor pressure-temperature relation [45].

Assumption (3) gives the other relation for gas phase pressures:

$$p_a^* = P_{total}^* - P_v^*.$$ (3.11)

The above three governing equations and five correlations can be used to solve the following eight unknown: $\rho_v, \rho_a,$ $\epsilon_\beta, \epsilon_\gamma,$ T, $\Gamma,$ $p_v, p_a.$ The effort required to solve the coupled transport equation is significant, although the numerical methods to solve these equations are well known. What appears to be extremely difficult is that special models need to be constructed so that the various transport stages in the problem can be studied properly, and comparison of the theoretical model with experiments in order to determine the parameters that appear in the transport equations. The general mathematical description of transport process needs to be extended to a series of specified theories that adequately describe the whole heat and mass transport process. Also we need some theoretical and experimental basis for estimating the values of the parameters which appear in the transport equations.

Chapter 4

QUASI-STEADY ANALYTICAL MODEL

4.1 Background

Experimental studies [23, 24] have shown that after a short initial transient period, the energy and vapor transfer processes reach a quasi-steady state. The numerical simulations by Tao et al. [38] have shown that quasi-steady conditions are reached within about one hour for practical situations. During this quasi-steady phase, heat flux and therefore the effective thermal conductivity attain high values.

In this section a detailed analysis is developed for energy transfer during the quasi-steady phase. Expressions for heat flux and effective thermal conductivity are derived for the flat-slab system. These are easily extended to a round-pipe system by a simple transformation of coordinates.

4.2 Analysis

A schematic diagram of the slab is shown in Fig. 1.1. The outer surface of the insulation is exposed to warm humid ambient air from which heat and water vapor flow towards the cold surface. These flows are caused by the temperature and vapor pressure gradients within the insulation. When the local vapor concentration at a point exceeds the saturation concentration corresponding to the local temperature, condensation occurs. The wet region is established and separated from dry region by the wet-dry interface. The vapor that reaches the impermeable surface condenses at this surface.

22

In addition to the basic assumptions made in Chapter Three, the following assumptions are made in the analytical model.

(1) The liquid phase is immobile and its effect on properties such as the vapor diffusion coefficient and the thermal conductivity is negligible. Since the quasi-steady state is reached in a short time (about an hour) for practical situations [38], the quantity of liquid condensed is relatively small, and it will therefore have little effect on the properties.

(2) All properties are independent of temperature. This assumption is justified because the temperature range of the present study is limited to about $0\text{-}40^\circ C$. The properties of the slab are therefore, evaluated at the mean temperature.

(3) The initial adsorption process is not taken into account because of its relatively small contribution to the total liquid fraction; only the liquid accumulation due to condensation in the wet-region is considered.

Subject to the above assumptions, the governing equations of energy and mass transfer for the quasi-steady state may be written as:

$$k^* \frac{d^2 T}{dx^2} + \Gamma h_{fg} = 0,$$ (4.1)

and

$$\rho_a^* D_v^* \frac{d^2 m}{dx^2} - \Gamma = 0.$$ (4.2)

In the dry region the condensation rate $\Gamma = 0$ and Equations (4.1) and (4.2) are uncoupled. In the wet region the vapor concentration m is a function of the local temperature.

The boundary conditions at the exposed surface, $x = 0$, of the slab are:

$$-k^* \frac{dT}{dx} = h^*[T_a - T(0)],$$ (4.3)

and

$$- \rho_a^* D_v^* \frac{dm}{dx} = h_m^* [m_a - m(0)].$$ (4.4)

At the impermeable surface, $x = L$, the boundary conditions are:

$$T(L) = T_2 \quad and \quad m_2 = g(T_2).$$ (4.5)

4.3 Nondimensional Form

In order to generalize the equations, the following nondimensional variables are introduced.

$$
\left.
\begin{aligned}
\textit{Dimensionless distance,} &\qquad z \;=\; \frac{X}{L} \\[2.5ex]
\textit{Dimensionless temperature,} &\qquad \theta \;=\; \frac{T-T_2}{T_a-T_2} \\[2.5ex]
\textit{Dimensionless concentration,} &\qquad C \;=\; \frac{m-m_2}{m_a-m_2} \\[2.5ex]
\textit{Heat transfer Biot number,} &\qquad B \;=\; \frac{h^*L}{k^*} \\[2.5ex]
\textit{Mass transfer Biot number,} &\qquad B_m \;=\; \frac{h_m^*L}{\rho_a^*D_v^*} \\[2.5ex]
\textit{Dimensionless condensation rate,} &\qquad G \;=\; \frac{\Gamma L}{\rho_a^*D_v^*(m_a-m_2)/L} \\[2.5ex]
\textit{Dimensionless heat flux,} &\qquad q \;=\; \frac{\bar{q}L}{k^*(T_a-T_2)} \\[2.5ex]
\textit{Dimensionless vapou flux,} &\qquad \Phi \;=\; \frac{\bar{\Phi}L}{\rho_a^*D_v(m_a-m_2)} \\[2.5ex]
\textit{Ratio of latent heat to conductive heat,} &\qquad \beta \;=\; \frac{\rho_a^*D_v^*h_{fg}(m_a-m_2)}{k^*(T_a-T_2)}.
\end{aligned}
\right\}
\qquad (4.6)
$$

The meaning of the symbols is defined in the Nomenclature.

The governing equations in terms of the dimensionless variables are:

$$
\frac{d^2\theta}{dz^2} + G\beta = 0, \tag{4.7}
$$

and

$$
\frac{d^2C}{dz^2} + G = 0. \tag{4.8}
$$

The boundary conditions become: at $z = 0$,

$$-\frac{d\theta}{dz} = B[1 - \theta(0)],$$ (4.9)

and

$$-\frac{dC}{dz} = B_m[1 - C(0)];$$ (4.10)

at $z = 1$,

$$\left. \begin{array}{rcl} \theta(1) & = & 0, \\ \\ C(1) & = & 0. \end{array} \right\}$$ (4.11)

4.4 Solution Procedure

4.4.1 Dry Region

The solution of Equations (4.7) and (4.8) in the dry-region are obtained by setting the condensation rate $G = 0$ and using the following conditions at the wet-dry interface. At $z = z_d$,

$$\left. \begin{array}{rcl} \theta(z_d) & = & \theta_c, \\ \\ C(z_d) & = & C_c. \end{array} \right\}$$ (4.12)

The expressions for the temperature and concentration in the dry region are as follows:

$$\theta(z) = \frac{-[1 - \theta_c]z + [\theta_c/B + z_d]}{[z_d + 1/B]},$$ (4.13)

and

$$C(z) = \frac{-[1 - C_c]z + [C_c/B_m + z_d]}{[z_d + 1/B_m]}.$$ (4.14)

4.4.2 Wet Region

Eliminating the condensation rate G between Equations (4.7) and (4.8), the total energy equation can be obtained as:

$$\frac{d^2\theta}{dz^2} + \beta\frac{d^2C}{dz^2} = 0, \qquad (4.15)$$

where β is a nondimensional group which may be interpreted as the ratio of latent heat transfer due to vapor flow to that of sensible heat transfer.

Since in the wet region the vapor is saturated, the vapor concentration is a unique function of local temperature, $C = f(\theta)$; the form of the function $f(\theta)$ will be given later in this section. Therefore, Equation (4-15) can be directly integrated to obtain the temperature distribution in the wet region as

$$\theta + \beta C(\theta) = b_1 z + b_2, \qquad (4.16)$$

where the concentration C is a function of the local temperature, b_1 and b_2 are constants of integration.

The following boundary and interface conditions are used to obtain b_1 and b_2.

$$\left.\begin{aligned} z = z_d, \quad \theta = \theta_c, \quad and \quad C = f(\theta_c); \\[2mm] z = 1, \quad \theta = 0, \quad and \quad C = 0. \end{aligned}\right\} \qquad (4.17)$$

This gives the temperature distribution in the wet-region as:

$$\theta + \beta f(\theta) = [\theta_c + \beta f(\theta_c)](\frac{1-z}{1-z_d}) \qquad (1 \le z \le z_d). \qquad (4.18)$$

4.4.3 Wet-Dry Interface

Both temperature distributions given by Equation (4.13) for the dry region and Equation (4.18) for the wet region contain two unknowns, θ_c and z_d. This requires a careful study of the wet-dry interface.

At the dry-wet interface the concentration, $C = f(\theta)$, therefore we have:

$$\frac{dC}{dz}\mid_c = f'(\theta)\frac{d\theta}{dz}\mid_c .$$

(4.19)

Substituting in Equation (4.19) for $\frac{d\theta}{dz}$ and $\frac{dC}{dz}$ from Equations (4.13) and (4.14), the following expression is obtained for the dry region length z_d

$$z_d = \frac{[1 - f(\theta_c)]/B - [f'(\theta_c)(1 - \theta_c)]/B_m}{[f'(\theta_c)(1 - \theta_c) - (1 - f(\theta))]}.$$

(4.20)

By applying the following interface condition:

$$\frac{d\theta}{dz}\mid_{wet} = \frac{d\theta}{dz}\mid_{dry},$$

(4.21)

this gives the equation

$$\frac{[\theta_c + \beta f(\theta_c)]}{(1 - z_d)[1 + \beta f'(\theta_c)]} = \frac{(1 - \theta_c)}{z_d + 1/B}.$$

(4.22)

Therefore

$$\frac{1 - z_d}{z_d + 1/B} = \frac{\theta_c + \beta f(\theta_c)}{[1 + \beta f'(\theta_c)](1 - \theta_c)}.$$

(4.23)

Substituting for z_d from Equation (4.20) in Equation (4.23), the following nonlinear equation is obtained for the interface temperature θ_c.

$$(1 - \theta_c) = \frac{(1 + 1/B)}{(1 + 1/B_m)}\frac{[1 - f(\theta_c)]}{f'(\theta_c)} + (\frac{1}{B} - \frac{1}{B_m})[\frac{\theta_c + \beta f(\theta_c)}{1 + \beta f'(\theta_c)}].$$

(4.24)

The function $f(\theta)$ in Equation (4.24) is the temperature dependence of the saturation concentration. In dimensional form this is given by

$$g(T) = a \exp[b(\frac{1}{T_0} - \frac{1}{T})], \tag{4.25}$$

which is the Clausius - Clapeyron relation.

The values of the constants a, b, and T_0 for the temperature range $0 \sim 58°C$ are [23]:

$$a = 0.0232, \qquad b = 5271.2, \qquad and \quad T_0 = 302K.$$

In nondimensional terms, Equation (4.25) has the form

$$f(\theta) = \frac{a \exp[b(\frac{1}{T_0} - \frac{1}{\theta(T_a - T_2) + T_2})]}{m_a - m_2} - \frac{m_2}{m_a - m_2}. \tag{4.26}$$

Note that at the impermeable surface, $\theta = 0$, and $f(\theta) = 0$.

An examination of Equation (4.24) shows that θ_c depends on three nondimensional numbers B, B_m and β. However, Equation (4.26) reveals that $f(\theta_c)$ depends on the operating conditions T_a, T_2 and m_a. When these variables are specified, the solution of Equation (4.24) for the unknown θ_c is easily accomplished by a trial and error procedure. Once θ_c is found, all the important heat transfer parameters can be obtained directly.

4.4.4 Trial and Error Procedure

The trial and error procedure for solving the interface temperature θ_c is as following:

1). Assuming an initial value for the dry-wet interface temperature θ_c, the local saturated vapor concentration and its first derivation are obtained from the Clausius-Clapeyron relationship. These values are substituted into Equation (4.20) to obtain the dry region length z_d.

2). Applying the boundary condition $\theta = \theta_2$ at the cold plate, one can obtained the wet region length from Equation (4.18).

3). The total slab length L is the sum of dry and wet region lengths. The computed slab length L is compared with the actual slab length.

4). If the computed slab length does not match the actual slab length, the θ_c value is adjusted and the procedure from step 1 to 3 is repeated until the computed slab length matches the actual slab length.

4.5 Heat Transfer

4.5.1 Heat Flux at Cold Plate

The heat flux at the cold surface is given by

$$\bar{q}_L = -[k^* \frac{dT}{dx} + h_{fg} \rho_a^* D_v^* \frac{dm}{dx}]_{x=L}. \tag{4.27}$$

It should be noted that the heat flux includes both sensible heat transfer and the latent heat released at the impermeable surface due to condensation.

Using Equations (4.18) and (4.20), the dimensionless heat flux is obtained as:

$$q_L = -\frac{[\theta_c + \beta f(\theta_c)][(1 - f(\theta_c)) - f'(\theta_c)(1 - \theta_c)]}{[(1 + 1/B_m)f'(\theta_c)(1 - \theta_c) - (1 + 1/B)(1 - f(\theta_c))]}. \tag{4.28}$$

4.5.2 Effective Thermal Conductivity

The equivalent thermal conductivity of the slab in the presence of condensation is defined by the same expression that is used for a dry slab. This is given by

$$\bar{q}_L(\frac{1}{h^*} + \frac{L}{k_{eff}}) = (T_a - T_2). \tag{4.29}$$

In the nondimensional form

$$q_L[\frac{1}{B} + (\frac{k_{dry}}{k_{eff}})] = 1. \tag{4.30}$$

Substituting for q_L in Equation (4.30) gives the following expression for (k_{eff}/k_{dry}) in terms of θ_c:

$$\frac{k_{eff}}{k} = \frac{[\theta_c + \beta f(\theta_c)][1 - f(\theta_c) - f'(\theta_c)(1 - \theta_c)]}{[\theta_c + \beta f(\theta_c) - (1 + 1/B_m)]f'(\theta_c)(1 - \theta_c) - [\theta_c + \beta f(\theta_c) - (1 + 1/B)(1 - f(\theta_c))]}. \tag{4.31}$$

4.6 Round-Pipe Insulation

For the round-pipe insulation system shown in Fig. 4.1 , moisture diffusion is assumed to occur uniformly across the circumference of the cross-section. Making the same assumptions as for the flat-slab, the governing equations of heat and vapor transfer can be written as:

$$\frac{d}{dr}[rk^*\frac{dT}{dr}] + h_{fg}r\Gamma = 0, \tag{4.32}$$

and

$$\frac{d}{dr}[r\rho_a^* D_v^*\frac{dm}{dr}] - r\Gamma = 0. \tag{4.33}$$

Consider the transformation:

$$y = r_0 \ln[\frac{r_0}{r}], \tag{4.34}$$

where r_0 is the outer radius of the insulation. Applying the transformation (4.34), Equations (4.32) and (4.33) become

$$\frac{d}{dy}[k^*\frac{dT}{dy}] + h_{fg}\Gamma(\frac{r}{r_0})^2 = 0, \tag{4.35}$$

Wet-dry Interface

$$\mathbf{T_a, \ M_a, \ h, \ h_m}$$
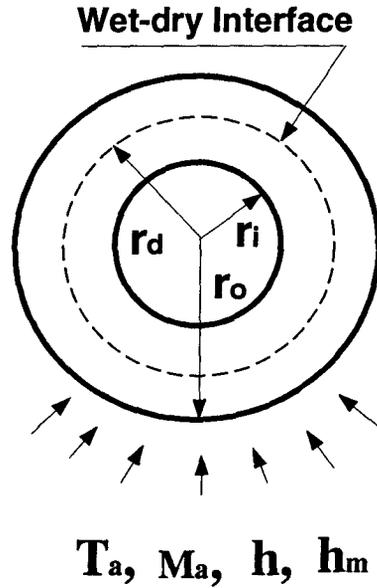
Figure 4.1: Schematic Diagram of Round-Pipe Insulation.

and

$$\frac{d}{dy}[\rho_a^* D_v^* \frac{dm}{dy}] - \Gamma(\frac{r}{r_0})^2 = 0. \tag{4.36}$$

The boundary conditions at the outer surface in the transformed system are:

at $r = r_0$, i.e $y=0$

$$k^* \frac{dT}{dy} = h^*[T_a - T(0)], \tag{4.37}$$

and

$$\rho_a^* D_v^* \frac{dm}{dy} = h_m^*[m_a - m(0)]. \tag{4.38}$$

It can be seen that in the dry region where $\Gamma = 0$, Equations (4.35) and (4.36) are the same as for a flat-slab as are the boundary conditions (4.37) and (4.38). In the wet-region the combined energy equation obtained by eliminating $\Gamma(\frac{r}{r_0})^2$ between Equations (4.35) and (4.36) is the same as Equation (4.15). Therefore it is clear that the final expressions

derived for the heat flux and effective thermal conductivity for flat slab can be applied to round-pipe insulations by taking the equivalent flat-slab thickness as

$$L_{eq} = r_0 \ln(\frac{r_0}{r_i}) \qquad (4.39)$$

where r_i is the inner radius of insulation.

4.7 Concluding Remarks

The analytical expressions for temperature distribution, heat flux and effective thermal conductivity in the presence of moisture gain have been derived. The main design and operating parameters on which the effective thermal conductivity depends are identified. The results of the parametric study using the above expressions and the verification of the model will be presented in the next Chapter.

Chapter 5

ANALYTICAL RESULTS AND DISCUSSIONS

5.1 Introduction

The quasi-steady model presented in the previous chapter was used to perform a detailed parametric study. It is useful to examine carefully the variables on which the heat flux and the effective thermal conductivity depend. The main dimensionless groups involved are B, B_m and β. The Lewis number for heat and mass transfer at outer surface may be assumed to be approximately unity [39]. With this assumption the dimensionless groups depend on three basic characteristics of the insulation viz. the thermal conductivity, the porosity and the thickness. The other variable is the outside heat transfer coefficient. The parameter β and the function $f(\theta)$, depend on the ambient temperature, the ambient relative humidity and the cold surface temperature.

In view of the above seven independent design and operating variables involved, it is difficult to represent the results in the most general form. Therefore for ease of application the results are presented in dimensional form, covering ranges of parameters that are of practical interest.

5.2 Comparison with Experimental Results

The predictions made by the analytical model derived in previous chapter for the heat flux and temperature distribution were compared with the experimental data presented in Ref. [23] for a flat-slab. The comparison of the measured [23] and computed temperature

34
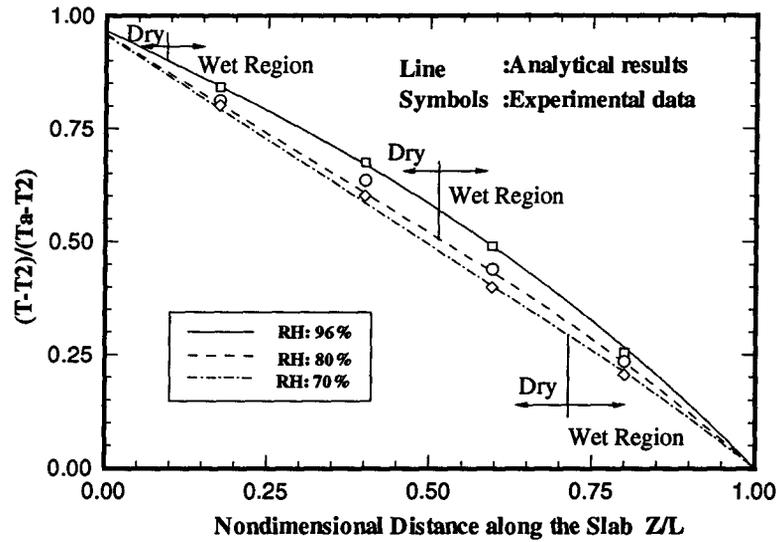
Figure 5.1: Temperature distribution in slab; Comparison with experimental Data [23].

T_a (°C)	T_{cold} (°C)	Relative Humidity (%)	Heat Flux Measured (W/m²)	Heat Flux Predicted (W /m²)
33.0	6.8	96	35.0	38.46
32.0	6.8	90	32.0	34
33.1	6.8	80	30.2	32.95
33.2	6.8	70	27.4	29.56

Table 5.1: Comparison of Predicted and Measured [23] Heat Flux

distribution is shown in Fig. 5.1. The conditions are as following: $T_a = 30°C$, $T_2 = 6.8°C$, dry density of insulation slab $\rho^* = 53$ kg/m³, $L = 66$ mm, and the relative humidities are 96%, 80% and 70% respectively. The computed temperature distributions agree well with the measurements. The computed wet-dry interface is also indicated in the figure.

The comparison of the computed and measured heat flux at the cold plate is shown in Table 5.1. There is satisfactory agreement between the calculated and measured heat flux.
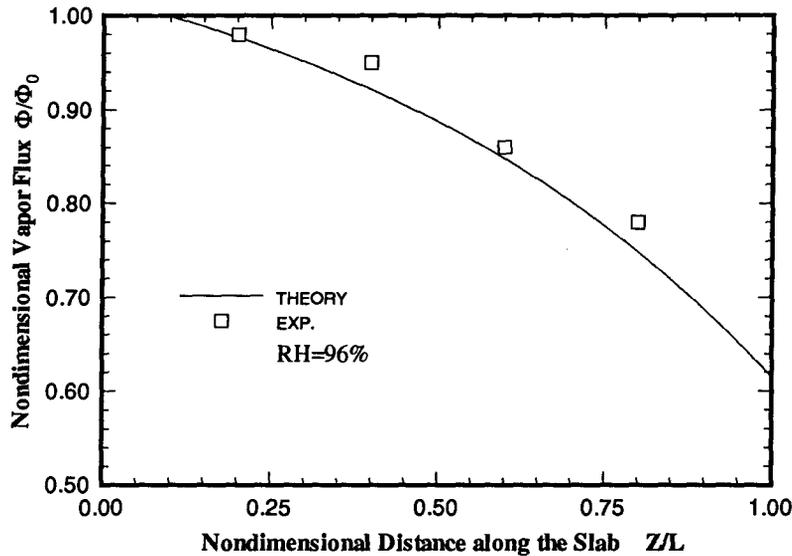
Figure 5.2: Vapor Flux Distribution in slab, Comparison with experimental data [23].

The comparison of predicted and measured vapor flux in the slab is shown in Fig. 5.2. The conditions are the same as in Fig. 5.1.

5.3 Comparison with Literature Reports

Figure 5.3 shows a comparison of the predicted heat flux using the present analytical model with the numerical results of Tao et al. [38]. The nondimensional heat flux was defined by Tao et al. [38] as the ratio of sensible heat flux with condensation in the slab to the dry-state heat flux with the same temperatures across the slab. This heat flux is shown as Q' in Fig 5.4. The slight discrepancy between the results can be attributed to the physical properties used. The present analytical model assumes constant mean physical properties while the numerical model [38] uses variable properties that depend on the liquid content.

In the present study the heat flux at the cold plate was defined by Equation (4.29) .
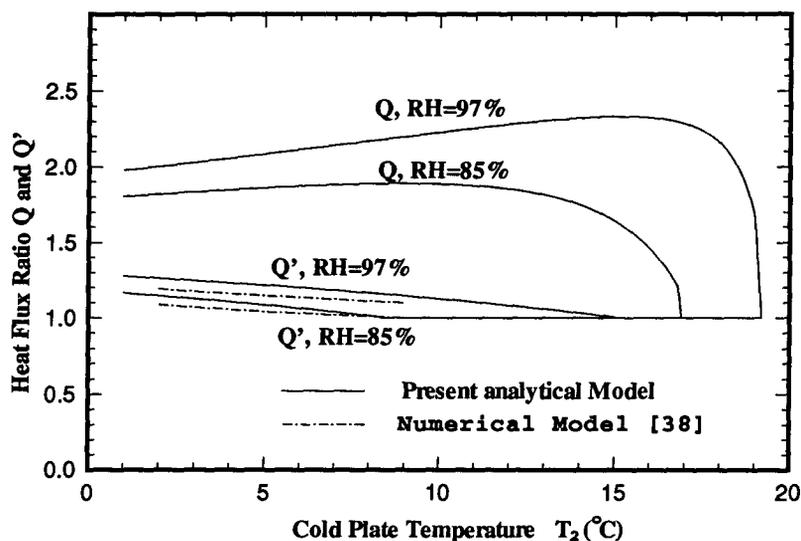
Figure 5.3: Comparison of analytical and numerical results, Conditions: $L = 0.099$ m, $T_a = 20°C$, $k_{dry} = 0.037$ W/m K, $h^* = 12$ W/m^2 K.

This includes the sensible heat flux and the latent heat released by the vapor condensing at the cold plate. The variation of the nondimensional total heat flux is indicated as Q in Fig. 5.3. It is seen that the magnitude of Q is more than twice that of Q'. The variation of the total heat flux with cold surface temperature will be discussed later in this section.

Modi and Benner [21, 22] measured the effective thermal conductivity of flat-slab insulations for different relative humidities and two values of the cold surface temperature. There is considerable scatter in their experimental data. However, there is an identifiable quasi-steady regime in the graphs. The quasi-steady values of the measured, and computed values of (k_{eff}/k_{dry}) are given in Table 5.2. There is satisfactory agreement when the cold surface temperature is $3°C$, but for a cold surface temperature of $10°C$ there is some disagreement.

T_a (°C)	T_{cold} (°C)	Relative Humidity (%)	k_{eff}/k_{dry} Measured	k_{eff}/k_{dry} Predicted
30	3	70	2.22	2.37
30	3	50	1.75	1.807
30	3	30	1.375	1.285
30	10	70	1.72	2.50
30	10	50	1.4	1.72
30	10	30	1.0	1.02

Table 5.2: Comparison of Predicted and Measured [21,22] Effective Thermal Conductivity

5.4   Effects of Condensation on Heat Transfer

The variation of the heat flux with the temperature difference is shown in Figs. 5.4-5.6, for different values of the ambient relative humidity and slab thickness.

The variation of the (k_{eff}/k_{dry}) with the temperature difference is shown in Figs. 5.7 - 5.9, for different values of the ambient relative humidity and slab thickness.

It is instructive to explain in physical terms the shape of these curves. Consider a practical situation where the ambient temperature and the ambient humidity are maintained constant and the cold surface temperature is decreased progressively starting from a value close to the ambient temperature. When the cold surface temperature T_2 is such that the saturation concentration, $m(T_2) \geq m_a$, the vapor concentration in the ambient, no vapour diffusion will occur. The value of (k_{eff}/k_{dry}) is then equal to unity and the heat flux is only due to sensible heat transfer. When $m(T_2) < m_a$, vapour will diffuse through the dry slab and condense at the cold surface. This small quantity of condensed liquid may be assumed to have negligible influence on the transport processes in the porous slab. The heat flux leaving the impermeable cold surface will include both the sensible heat flux and the latent heat flux due to condensation. The heat flux at the cold surface increases with the temperature difference due to the increased sensible heat
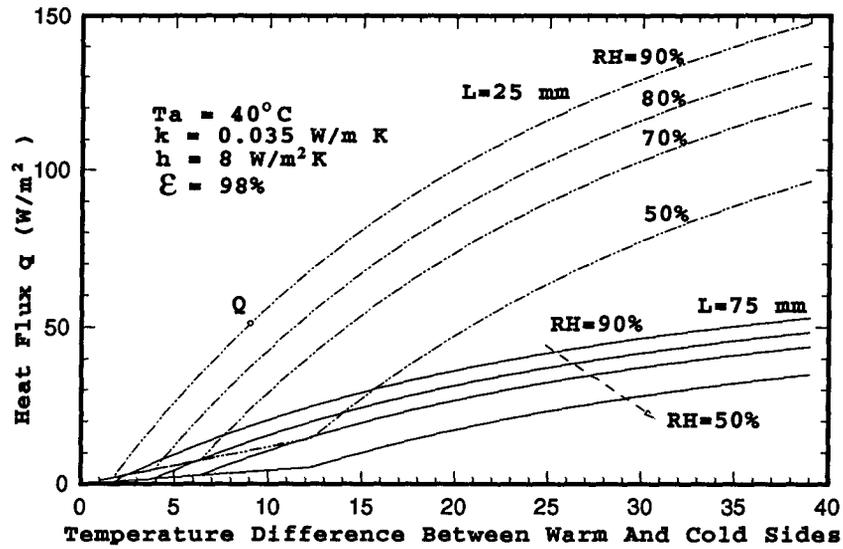
Figure 5.4: Variation of heat flux with temperature difference, $T_a = 40^\circ C$.
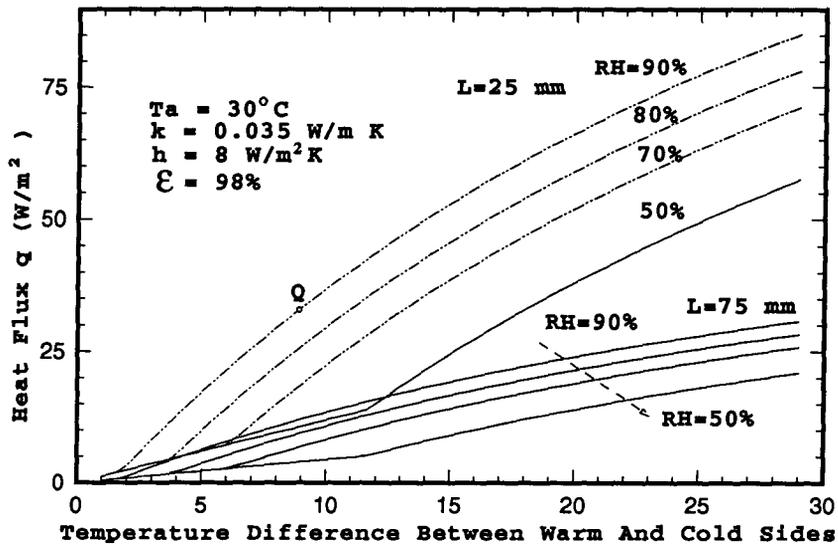
Figure 5.5: Variation of heat flux with temperature difference, $T_a = 30^\circ C$.
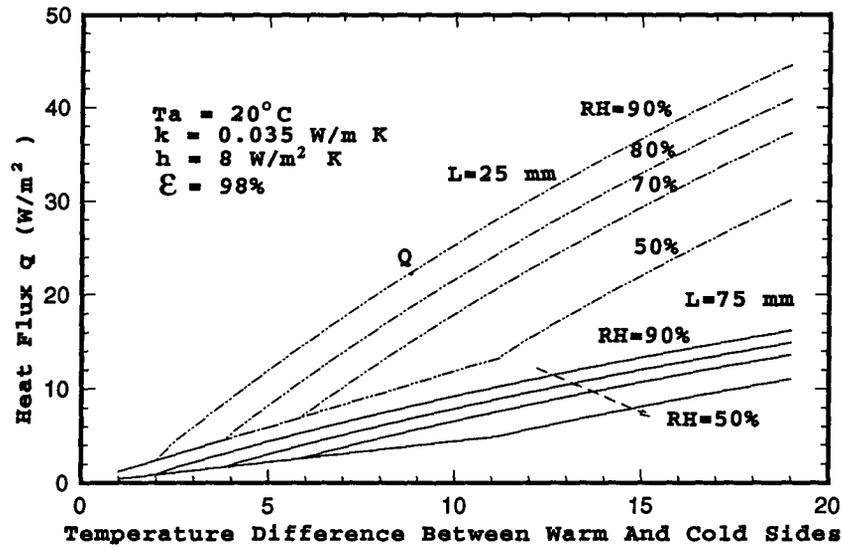
Figure 5.6: Variation of heat flux with temperature difference, $T_a = 20^\circ C$.
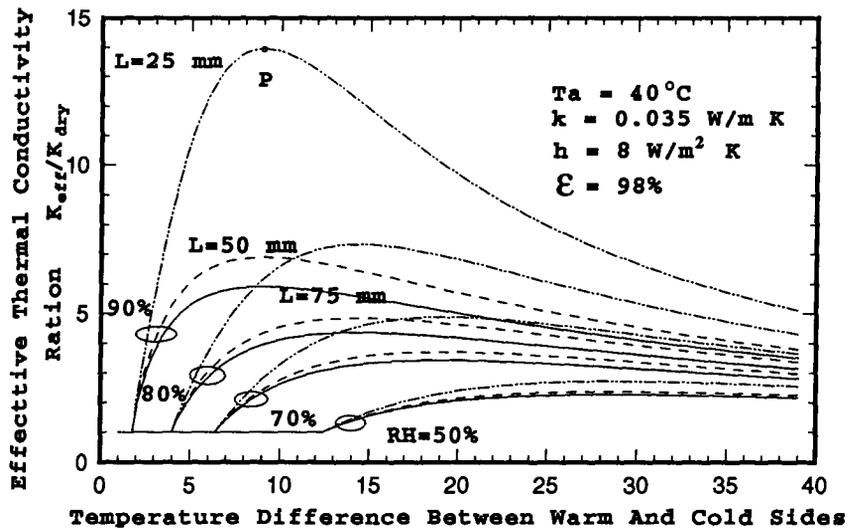
Figure 5.7: Variation of effective thermal conductivity ratio with temperature difference, $T_a = 40^\circ C$.
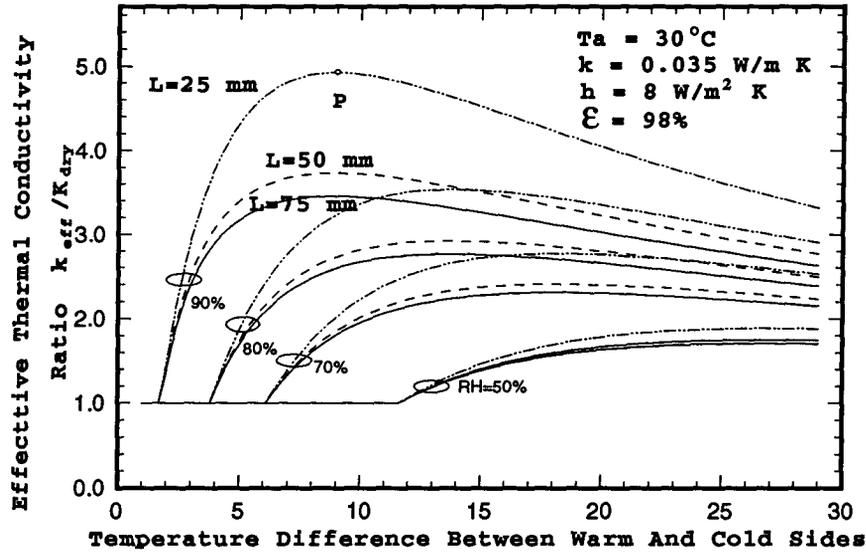
Figure 5.8: Variation of effective thermal conductivity ratio with temperature difference, $T_a = 30^\circ C$.

transfer and the increased vapour flux. The ratio (k_{eff}/k_{dry}) also increases due to the same reason.

At the turning point P in Fig. 5.7 and the corresponding point Q in Fig. 5.4, the vapour condensation is just beginning to occur within the insulation slab. At this point the wet-dry interface is just at the cold surface and the dry length z_d given by Equation (4.20) is equal to one. When the temperature difference is increased further, the wet-dry interface moves towards the exposed surface i.e. z_d decreases progressively. Figures. 5.4-5.6 show that the heat flux increases continuously with increasing temperature difference. However, the rate of increase of the total heat flux is reduced because of the decrease in the function $f'(\theta)$ with temperature. Due to the different rates of variation of $\bar{q}$ and $(T_a - T_2)$, the value of (k_{eff}/k_{dry}) increases up to P and then decreases slowly.

The definition of k_{eff} is based on Equation (4.29), which is the design energy equation
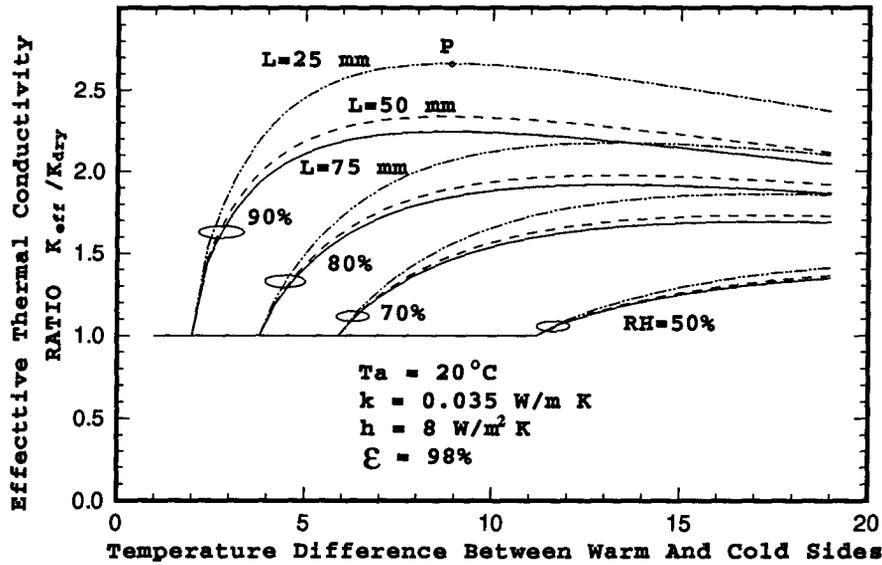
Figure 5.9: Variation of effective thermal conductivity ratio with temperature difference, $T_a = 20°C$.

for dry insulation systems. This definition facilitates the inclusion of the effects of condensation in more broader energy conservation studies by the use of a modified thermal conductivity value. This definition, however, leads to the somewhat unusual variation of k_{eff} with temperature difference as discussed earlier.

The heat flux and the effective thermal conductivity increase with decreasing slab thickness. As expected higher ambient temperatures and humidities lead to higher effective thermal conductivities.

The sensitivity of the effective thermal conductivity to the heat transfer coefficient, the thermal conductivity and porosity of the insulation is shown in Figs. 5.10, 5.11 and 5.12 respectively. Its magnitude increases with decreasing h_a and k and increasing porosity.

Design data for round-pipe insulations may be easily deduced from Figs. 5.7-5.9 using
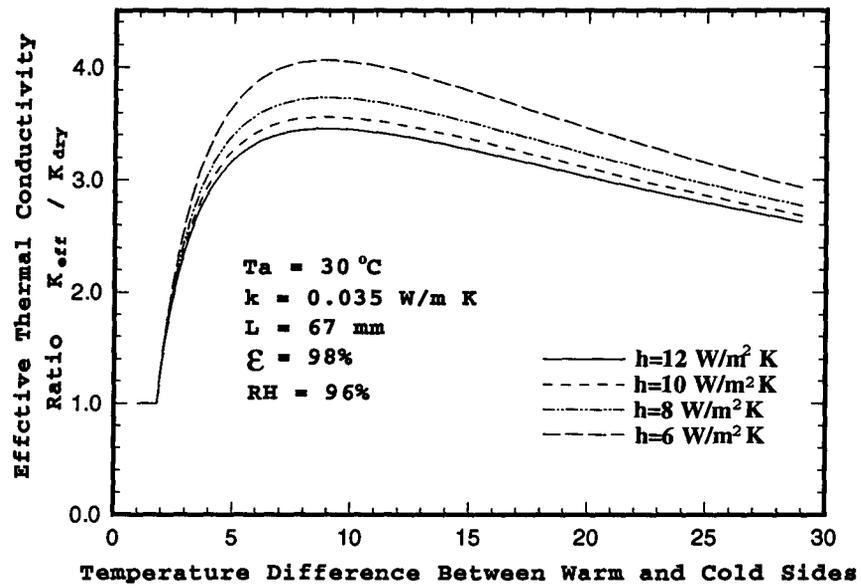
Figure 5.10: Effect of h on the variation of the effective thermal conductivity ratio.
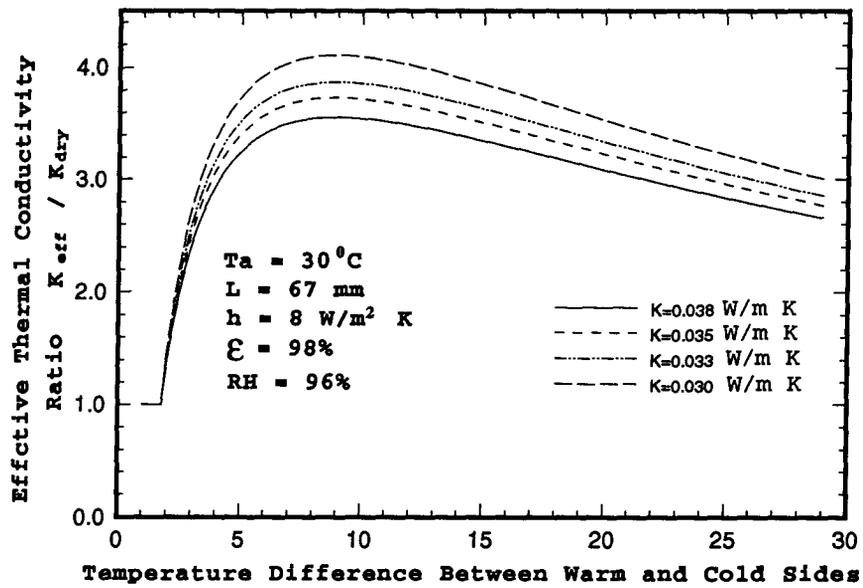
Figure 5.11: Effect of K on the variation of the effective thermal conductivity ratio.
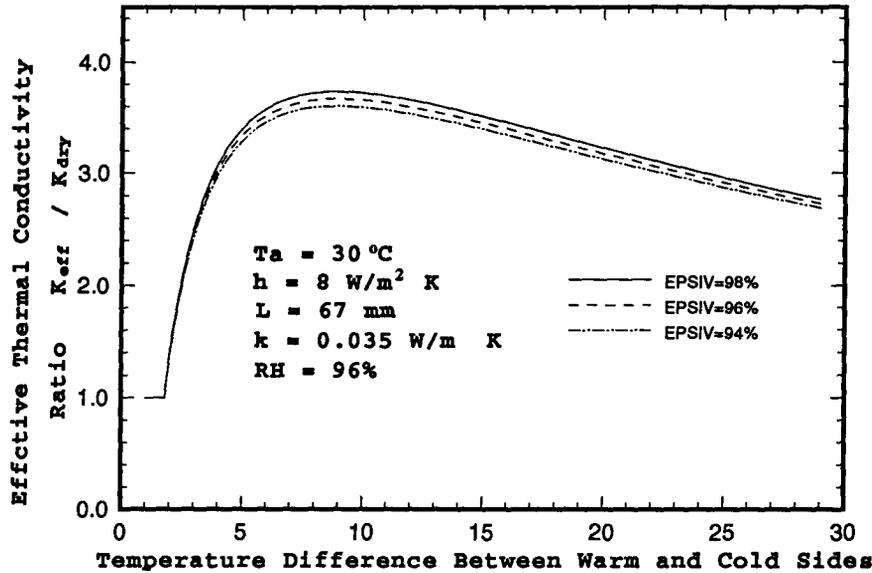
Figure 5.12: Effect of ϵ on the variation of the effective thermal conductivity ratio.

the equivalent flat-slab length given by Equation (4.39). For example, a 35 mm thick pipe insulation applied on a pipe of diameter 50 mm has an equivalent flat-slab thickness of about 52.5mm. The curves in Figs. 5.7-5.9 may now be used to find the effective thermal conductivity for $L = 52.5$ mm.

5.5 Concluding Remarks

An analytical model is developed for the quasi-steady phase of the heat and water vapor transfer through flat and pipe insulations. The computational effort involves the solution of the nonlinear equation (4.18), by a trial and error method, to determine the dimensionless temperature θ_c at the wet-dry interface. With a knowledge of θ_c, the heat flux and the effective thermal conductivity are obtained by directed substitution in Equation (4.28) and (4.31) respectively. The same procedure is appliable for pipe insulations with

the use of the equivalent flat slab thickness given by Equation (4.39).

The effective thermal conductivity and the heat flux in the presence of condensation depend on seven independent design and operating variables of system.

The effective thermal conductivity increases with increasing temperature difference across the insulation and reaches a maximum when condensation begins to occur in the slab. Thereafter, it decreases slightly as the temperature difference is increased further. For practical operating conditions the effective thermal conductivity varies from about 1.5 to 15 times the dry-state value.

The results of the parametric study are presented as curves which may be used to estimate the effective thermal conductivity over practical conditions for design purposes. The same curves can be used for pipe insulations with the use of equivalent flat-slab thickness.

Chapter 6

TRANSIENT NUMERICAL MODEL

6.1 Introduction

The moisture transport processes in this physical model have four main stages which have been stated in Chapter One. There is an initial transient period which may last up to about an hour for most practical situations before a quasi-steady phase is attained. The quasi-steady state may last anywhere up to several days before the accumulation and transport of liquid water begins to significantly affect the heat transfer due to reevaporation and changes in physical properties of the insulation. The quasi-steady analytical model presented in Chapter Four has given reasonable prediction of the heat and mass transfer parameters for the quasi-steady phase. However, many simplifying assumptions have been made in order to obtain the quasi-steady solutions. For numerical studies on transient moisture transfer through porous insulation, only work on the effect of condensation during the early time period has been reported in the literature [35-37]. In this Chapter, the long-term transient moisture transport processes are analyzed, and the significant transport mechanisms are identified. Accordingly, the rigorous and detailed formulation of heat and moisture transfer for all the stages is presented. The long term effects of condensation are investigated numerically, and the mobile condensate is taken into account.

6.2 Analysis and Formulation

6.2.1 General Formulation

The assumptions made in the transient formulation are the same as that stated in Chapter Three. The formulation is based on the local volume-averaged technique. In order to generalize the mathematical formulation, the following new set of nondimensional variables have been introduced:

$$
\left.
\begin{aligned}
Dimensionless \;\; distance, & \qquad z \;\; = \;\; \frac{X}{L} \\[2em]
Dimensionless \;\; temperature, & \qquad \theta \;\; = \;\; \frac{T}{T_a - T_2} \\[2em]
Dimensionless \;\; density, & \qquad \rho_i \;\; = \;\; \frac{\rho_i^*}{\rho_0^*} \\[2em]
Dimensionless \;\; time, & \qquad t \;\; = \;\; \frac{t^*}{L^2/\alpha_{0,eff}^*} \\[2em]
Dimensionless \;\; condensation \;\; rate, & \qquad G^* \;\; = \;\; \frac{\Gamma}{\rho_0^* \alpha_{0,eff}^* / L^2} \\[2em]
Dimensionless \;\; heat \;\; capacity, & \qquad c_p \;\; = \;\; \frac{c_p^*}{c_{p0}^*} \\[2em]
Dimensionless \;\; thermal \;\; conductivity, & \qquad k \;\; = \;\; \frac{k^*}{k_0^*} \\[2em]
Dimensionless \;\; vapor \;\; diffusivity, & \qquad D_v(\theta) \;\; = \;\; \frac{D_v^*(T)}{\alpha_{0,eff}^*} \\[2em]
Dimensionless \;\; liquid \;\; diffusivity, & \qquad D_\beta(w) \;\; = \;\; \frac{D_\beta^*(w)}{\alpha_{0,eff}^*}.
\end{aligned}
\right\} \qquad (6.1)
$$

The symbols are also defined in the Nomenclature.

The governing equations (3.3)-(3.5) in terms of the dimensionless variables are:

Vapor diffusion equation;

$$\frac{\partial}{\partial x}[D_v(\theta)\frac{\partial \rho_v}{\partial z}] - G^* = \frac{\partial(\epsilon_\gamma \rho_v)}{\partial t}, \tag{6.2}$$

Liquid transport equation;

$$\rho_\beta \frac{\partial}{\partial z}[D_\beta(w)\frac{\partial \epsilon_\beta}{\partial z}] + \frac{G^*}{P_1} = \frac{\partial \epsilon_\beta}{\partial t}, \tag{6.3}$$

Energy equation;

$$\frac{\partial}{\partial z}[k(w)\frac{\partial \theta}{\partial z}] + P_2 G^* = \rho c_p \frac{\partial T}{\partial t}. \tag{6.4}$$

The corresponding constitutive correlations in terms of the dimensionless variables are:

Volumetric Constraint;

$$\epsilon_\sigma + \epsilon_\beta + \epsilon_\gamma = 1, \tag{6.5}$$

Thermodynamic Relations;

$$p_v = P_3 \rho_v \theta, \tag{6.6}$$

$$p_a = P_4 \rho_a \theta, \tag{6.7}$$

$$p_v = Exp[P_5(\frac{1}{\theta} - \frac{1}{\theta_{ref}})], \tag{6.8}$$

and

$$p_{total} = p_a + p_v. \tag{6.9}$$

The dimensionless parameters are defined as the following:

$$
\left.\begin{aligned}
P_1 &= \frac{\rho_\beta^*}{\rho_0^*} \\[2em]
P_2 &= \frac{h_{fg}}{c_{p0}^* \Delta T} \\[2em]
P_3 &= \frac{\Delta T R_v \rho_v^*}{p_{v,0}^*} \\[2em]
P_4 &= \frac{\Delta T R_v \rho_v^*}{p_{v,0}^*} \\[2em]
P_5 &= \frac{h_{fg}}{R_v \Delta T}.
\end{aligned}\right\}
\tag{6.10}
$$

The spatial average density of porous insulation is defined as

$$
\rho = \epsilon_\sigma \rho_\sigma + \epsilon_\beta \rho_\beta + \epsilon_\gamma \rho_\gamma.
\tag{6.11}
$$

The mass fraction weighted average quantity of heat capacity is defined as

$$
C_p = \frac{\epsilon_\sigma \rho_\sigma c_{p,\sigma} + \epsilon_\beta \rho_\beta c_{p,\beta} + \epsilon_\gamma \rho_\gamma c_{p,\gamma}}{\rho}.
\tag{6.12}
$$

The problem is modeled as a porous insulation with impermeable and adiabatic vertical boundaries. The upper horizontal boundary is impermeable and subjected to a cold temperature, and the lower one is exposed to moist ambient at a warm and humid condition. The insulation slab is assumed to be fully dry and initially has a uniform temperature. It encounters a temperature drop at upper surface and is suddenly exposed to the ambient air at the lower surface.

Therefore, the initial condition for the model is

$$\left. \begin{array}{rcl} \rho_v(z,0) & = & \rho_{v,a} \\\\ \\ \epsilon_\beta(z,0) & = & 0 \\\\ \\ \theta(z,0) & = & \theta_a. \end{array} \right\} \tag{6.13}$$

The boundary conditions to complete the formulation are

$$\frac{\partial \theta}{\partial z} \Big|_{(0,t)} = B[\theta_a - \theta(0,t)], \tag{6.14}$$

$$\frac{\partial \rho_v}{\partial z} \Big|_{(0,t)} = B_m[\rho_{v,a} - \rho_v(0,t)], \tag{6.15}$$

$$\theta(1,t) = \theta_2, \tag{6.16}$$

$$\rho_v(1,t) = g(\theta_2), \tag{6.17}$$

where $g(\theta)$ is saturated vapor density which can be represented by the Clausius-Clapeyron relation

$$g(\theta) = exp[P_5(\frac{1}{\theta_2} - \frac{1}{\theta_{ref}})]/P_3\theta_2. \tag{6.18}$$

6.2.2 Stage 1: Initial Process

Initially, it is assumed that there is no water vapor condensate inside the insulation slab. The temperature and vapor density fields are governed by:

Vapor diffusion equation;

$$\frac{\partial}{\partial z}[D_v(\theta)\frac{\partial \rho_v}{\partial z}] = \epsilon_\gamma \frac{\partial \rho_v}{\partial t}, \tag{6.19}$$

Energy equation;

$$\frac{\partial}{\partial z}[k_d(\theta)\frac{\partial \theta}{\partial z}] = \rho c_p \frac{\partial \theta}{\partial t}, \tag{6.20}$$

where the dry thermal conductivity is the only thermal property which is a function of temperature. Although there might be some initial adsorbed water inside the slab in practical situations, it is assumed that the insulation slab is totally dry initially, and the liquid fraction is zero,

$$\epsilon_\beta = 0. \tag{6.21}$$

6.2.3 Stage 2: Immobile Liquid Accumulation

Stage 2 is identified as that when condensation occurs within the insulation slab. The air-vapor mixture is saturated when the actual vapor density in a region is larger than or equal to the local saturated vapor density which can be represented by equation (6.18). The new two-phase regions (dry-wet) are then determined and the wet-dry boundary is located where the actual vapor density is just equal to the local saturation vapor density. It should be noted physically, due to the inhomogeneities of actual fibrous insulation, the wet-dry boundary is not a single line but has a finite volume. However according to the local average technique, this fuzzy boundary volume can be averaged and represented by a line.

- Dry Region

    In the dry region, the condensation rate G^* is set to zero, as well as the liquid fraction for the above mentioned reasons. Equations (6.20)-(6.19) can be still used

for solving the temperature and vapor density fields.

- Wet Region

During this stage, the liquid which is accumulated due to condensation is small and has an insignificant effect on the properties. Therefore, the liquid is practically immobile, and is accumulated at a constant rate.

The temperature and vapor density fields are governed by Equations (6.2) and (6.3). Since the vapor is saturated in the wet region, vapor density is the only property which is a function of the local temperature, and it can be represented by the Clausius-Clapeyron relation (6.18).

Differentiating of Equation (6.18) against t and z respectively, one obtains:

$$\frac{\partial \rho_v}{\partial z}\bigg|_{wet} = g'(\theta)\frac{\partial \theta}{\partial z}, \tag{6.22}$$

and

$$\frac{\partial \rho_v}{\partial t}\bigg|_{wet} = g'(\theta)\frac{\partial \theta}{\partial t}. \tag{6.23}$$

Eliminating the condensation rate G^* between Equations (6.2) and (6.3), and making use of relations (6.22) and (6.23), the vapor diffusion equation (6.2) and energy equation (6.3) can be combined as:

$$[\rho c_p + P_2 \epsilon_\gamma g'(\theta)]\frac{\partial \theta}{\partial t} + P_2 g(\theta)\frac{\partial \epsilon_\gamma}{\partial t} = \frac{\partial}{\partial z}[(k(w) + P_2 D_v(\theta)g'(\theta))\frac{\partial \theta}{\partial z}]. \tag{6.24}$$

Together with boundary conditions on the cold side (6.16) and on the wet-dry interface, which will be stated later, Equation (6.24) can be used to solve for the temperature field in the wet region without the need to deal with an unknown source term. Once the temperature distribution in the wet region is known, the

saturated vapor density profile in the wet region can be obtained easily from Eq. (6.18), and the condensation rate can be solved either from the vapor diffusion equation (6.2) or the energy equation (6.3).

Since the liquid is in a pendulous state, the liquid diffusion equation (6.4) is reduced to

$$\frac{\partial \epsilon_\beta}{\partial t} = \frac{G^*}{P_1}.$$
(6.25)

6.2.4 Stage 3: Mobile Liquid Diffusion

When the amount of liquid has been collected to some extent, the liquid can no longer be trapped in the pores. The liquid will diffuse in the direction of liquid content gradient. Since all the vapor reaching the impermeable cold plate is considered to have condensed at the cold plate, the liquid fraction is highest near the cold plate at the beginning, and diffuses towards the warmer, and drier direction.

The critical liquid fraction $\epsilon_{\beta,cr.}$ denotes the liquid fraction below which the liquid is immobile. It is a complex function of the structure of fibers, liquid pressure, surface tension etc.. According to the experimental results of Cid and Crausse [28] for fibrous insulation with dry state density of $\rho_0^* = 53 \text{ kg/m}^3$, the liquid diffusivity abruptly becomes significant (about $10^{-7} \text{ m}^2/\text{s}$) when the liquid fraction is between 0.035-0.075.

After the liquid starts to flow, there are two situations to be distinguished. In the first case, the liquid diffuses inside the wet region. There is no apparent liquid front, the liquid diffusion equation is applied where the liquid fraction exceeds the critical value. In the second case, the liquid flows out the wet region. It enlarges the wet region and makes the wet-dry interface move due to the mobile liquid front.

The temperature and vapor density fields in the wet region are formulated in the same

way as that in stage 2. However, treatment of the moving wet-dry interface is needed for this stage, and will be stated in the section of solution methodology.

The Equation (6.4) was developed to govern the liquid diffusion. However, the liquid diffusivity is a phenomenological quantity. Without any available experimental data, the liquid diffusion coefficient is not a known quantity. Cid and Crausse [28] measured the liquid diffusion coefficient for several commonly used fibrous insulation. Their liquid diffusion coefficient $D_l(w)$ is defined as in the following liquid transport equation:

$$\frac{\partial w}{\partial t^*} = \frac{\partial}{\partial x}[D_l^*(w)\frac{\partial w}{\partial x} + \frac{\rho_\beta^*}{\rho_0^*}K(w)] + \frac{\Gamma}{\rho_0^*}. \tag{6.26}$$

where w is weight liquid content, $K(w)$ is hydraulic conductivity and is the function of the liquid saturation S. The relations between w, S and liquid fraction ϵ_β are

$$w = \frac{\rho_\beta^*}{\rho_0^*}\epsilon_\beta, \tag{6.27}$$

$$S = \frac{\rho_0^*}{\rho_\beta^*}\frac{w}{\epsilon_0}, \tag{6.28}$$

$$\epsilon_\beta = \epsilon_0 S = (1 - \epsilon_\sigma)S, \tag{6.29}$$

where ϵ_0 is the void fraction of porous insulation.

Note that some important relations exist between the differentiations of w, S, $K(w)$ and liquid fraction ϵ_β:

$$\frac{\partial K(w)}{\partial x} = \frac{\partial K(w)}{\partial w}\frac{\partial w}{\partial x}, \tag{6.30}$$

$$\frac{\partial K(w)}{\partial w} = \frac{\partial K(w)}{\partial S}\frac{\partial S}{\partial w} = \frac{1}{\epsilon_0}\frac{\rho_\beta^*}{\rho_0^*}\frac{\partial K(w)}{\partial S}, \tag{6.31}$$

$$\frac{\partial w}{\partial x} = \frac{\rho_\beta^*}{\rho_0^*} \frac{\partial \epsilon_\beta}{\partial x}, \tag{6.32}$$

$$\frac{\partial w}{\partial t^*} = \frac{\rho_\beta^*}{\rho_0^*} \frac{\partial \epsilon_\beta}{\partial t^*}. \tag{6.33}$$

Substituting the above relations into the Equation (6.26), the liquid diffusion equation with experimentally determined liquid diffusion coefficient, in terms of the liquid fraction, is obtained:

$$\frac{\partial \epsilon_\beta}{\partial t^*} = \frac{\partial}{\partial x}[D_l^*(\epsilon_\beta)\frac{\partial \epsilon_\beta}{\partial x}] + \frac{1}{\epsilon_0}\frac{\partial K(w)}{\partial S}\frac{\partial \epsilon_\beta}{\partial x} + \frac{\Gamma}{\rho_\beta^*}. \tag{6.34}$$

Applying the same dimensionless variables as in Eq. (6.1), the liquid diffusion equation in nondimensional form is

$$\frac{\partial \epsilon_\beta}{\partial t} = \frac{\partial}{\partial z}[D_l(\epsilon_\beta)\frac{\partial \epsilon_\beta}{\partial z}] + F(S)\frac{\partial \epsilon_\beta}{\partial z} + \frac{G^*}{P_1}, \tag{6.35}$$

where P_1 is defined in (6.10), and F(S) can be viewed as a coefficient due to hydraulic conductivity, and is defined as:

$$F(S) = \frac{1}{\epsilon_0}\frac{\partial K(w)}{\partial S}\frac{L}{\alpha_{0,eff}^*}. \tag{6.36}$$

The liquid diffusion coefficient and hydraulic conductivity in terms of the liquid saturation are regressed from Cid and Crausse's experimental data [28]. The following polynomials have less than 5% discrepancy from the original experimental data:

$$\begin{aligned} D_l^*(S) &= 1.29(10)^{-8} + 9.913(10)^{-7}S + 1.6018(10)^{-6}S^2 - 7.8408(10)^{-6}S^3 \\ &\quad + 1.053(10)^{-5}S^4; \qquad\qquad 0.45 \geq S \geq 0.05, \end{aligned} \left.\begin{aligned}&\\&\end{aligned}\right\} \tag{6.37}$$

$$
\begin{aligned}
K(S) \;=\;& 4.502(10)^{-7} - 4.658(10)^{-6}S + 1.05486(10)^{-3}S^2 - 2.56279(10)^{-3}S^{-3} \\
& -1.7555(10)^{-4}S^4 + 3.956(10)^{-3}S^5; \qquad 0.45 \ge S \ge 0.05.
\end{aligned}
\right\}
$$

$$(6.38)$$

6.2.5 Stage 4: Long Term Liquid Accumulation and Diffusion

The liquid front eventually reaches the exposed surface, the entire insulation slab becomes wet. The liquid is accumulated continuously because the water vapor from the ambient air keeps condensing inside the slab and on the cold plate. The liquid will move under the liquid fraction gradient, and will be redistributed continuously.

The formulation for this stages is quite the same as that for the wet region in previous stage except that convective boundary conditions are introduced into the formulation for the wet region. The treatment of these boundary conditions on the exposed surface will be stated in detail in the next section.

6.3 Solution Methodology

The above introduced formulation can not be solved analytically. The numerical scheme is based on the finite difference form of the above-stated formulation. The solution domain is divided into a finite number of control volumes or cells. A grid-point is placed at the geometric center of each control volume. This arrangement has the following advantages:

- The value of the general variable which is available at the center of the control volume represents the volume averaged value over the control volume.

- The physical properties and the source terms can be calculated at the center of the control volume.
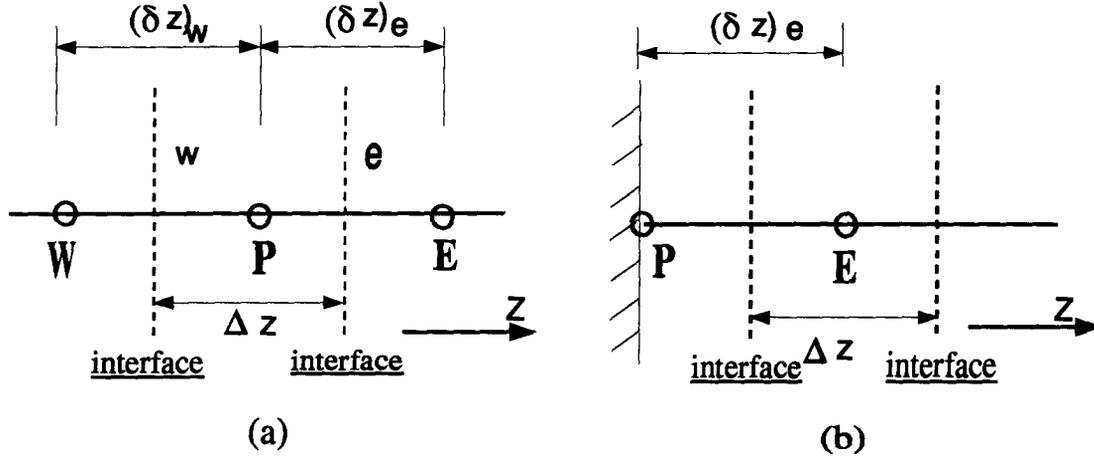
Figure 6.1: Grid-point Cluster for One Dimensional Transport Problem: (a). Control Volume for the Internal Points, (b). Control Volume for the Boundary Points.

- Discontinuities at the boundaries can be conveniently handled by locating boundary cells where the discontinuities occur.

6.3.1 Discretized Formulations

The discretized system of the governing equations is formed with a grid-point cluster shown in Fig. 6.1. The dashed line show the faces of the control volume. For the one-dimensional problem under consideration, we assume an unit thickness in the directions other than z. Modification of these control volumes near the boundaries is straightforward.

For the numerical purpose, the governing equations described in the previous section can be represented by the general transport equation

$$\frac{\partial}{\partial t}(\Phi) = \frac{\partial}{\partial z}[B(\frac{\partial \Phi}{\partial z})] + S_\Phi \tag{6.39}$$

where Φ can be replaced for different equations, B is a general diffusion coefficient, and S_Φ

a general source term. The discretized form of Equation (6.39) is obtained by integrating over the respective control volumes, i.e.,

$$\int_t^{t+\Delta t} \int_t^{t+\Delta t} \frac{\partial \Phi}{\partial t} dt dz = \int_t^{t+\Delta t} \int_t^{t+\Delta t} [\frac{\partial}{\partial z}(B(\frac{\partial \Phi}{\partial z}) + S_\Phi] dz dt. \qquad (6.40)$$

For detailed derivation method of the discretized equation, one could refer to Patankar's work [42]. The fully implicit scheme is chosen for the requirements of stability, simplity and physically satisfactory behavior. In general, the central difference form is used for internal nodes and the backward or forward difference used for the boundary nodes. The backward difference form is used for the time derivative. The discretized forms of the formulations for this problem are given as the following.

Stage 1: Initial Process

The discretized equation for energy transfer is:

at the internal nodes,

$$a_P \theta_P = a_E \theta_E + a_W \theta_W + b, \qquad (6.41)$$

where

$$a_E = \frac{k_e}{(\delta x)_e}, \qquad (6.42)$$

$$a_W = \frac{k_w}{(\delta z)_w}, \qquad (6.43)$$

$$a_P^0 = \frac{\rho c_p \Delta z}{\Delta t}, \qquad (6.44)$$

$$b = a_P^0 \theta_P^0, \qquad (6.45)$$

$$a_P = a_E + a_W + a_P^0. \qquad (6.46)$$

For the dry slab, the conductivity variation only depends on temperature distribution. The interface conductivities k_e, k_w in terms of these grid-point values are

$$k_e = \frac{2k_P k_E}{k_P + k_E},$$ (6.47)

$$k_w = \frac{2k_p k_W}{k_P + k_W}.$$ (6.48)

At $z = 0$, half cell near boundary is introduced, the boundary condition is

$$\frac{\rho c_p}{\Delta t} \frac{\Delta z}{2}(\theta_P - \theta_P^0) = \frac{k_e}{(\delta z)_e}(\theta_E - \theta_P) - h(\theta_P - \theta_a),$$ (6.49)

where h is dimensionless convective heat transfer coefficient in the ambient, and ϵ_γ is constant for a dry slab.

The vapor diffusion equation has a similar discretized form to that of the energy equation. The equation system (6.41)-(6.46) can be used for vapor diffusion, if the corresponding variable and coefficients are replaced. The boundary condition for the vapor diffusion equation at $z = 0$ is

$$\frac{\epsilon_\gamma}{\Delta t} \frac{\Delta z}{2}(\rho_{v,P} - \rho_{v,P}^0) = \frac{D_{v,e}}{\delta z}(\rho_{v,E} - \rho_{v,P}) - h_m(\rho_{v,P} - \rho_{v,a}),$$ (6.50)

where h_m is dimensionless mass transfer coefficient in the ambient.

At $z = 0$, the temperature at the cold plate is given; no problems are introduced in the discretized energy equation. The vapor density at this boundary is equal to the saturated vapor density at T_2.

Stage 2: Immobile Liquid Accumulation

In this stage, the discretization equations for the dry region are the same as that in stage one. For the wet region, the combined energy equation (6.24) can not be solved directly because the gas phase volume fraction ϵ_γ is not known. An iterative procedure is needed to solve for the temperature field in the wet region.

The first derivative term of ϵ_γ is omitted for the first iteration, the combined energy equation becomes

$$[\rho c_p + P_2\epsilon_\gamma g'(\theta)]\frac{\partial\theta}{\partial t} = \frac{\partial}{\partial z}[(k(w) + P_2 D_v(\theta)g'(\theta))\frac{\partial\theta}{\partial z}], \tag{6.51}$$

which has the following discretized form for the internal grids,

$$[\rho c_p + P_2\epsilon_\gamma g'(\theta)]_P\frac{\Delta z}{\Delta t}(\theta_P - \theta_P^0) = \left. \begin{array}{l} \frac{[(k(w)+P_2 D_v(\theta)g'(\theta))]_e}{\Delta z}(\theta_E - \theta_P) \\[2mm] \frac{[(k(w)+P_2 D_v(\theta)g'(\theta))]_w}{\Delta z}(\theta_P - \theta_W). \end{array} \right\} \tag{6.52}$$

In the dry-wet interface, the boundary condition for the combined energy equation can be derived from the energy balance at the interface. Assuming that the grid size can be taken fine enough so that the dry-wet interface is approximately located at the interface of control volumes, as shown in Fig. 6.2, the energy balance of the grid where the dry-wet interface locates can be written as

$$[\rho c_p + P_2\epsilon_\gamma g'(\theta)]_P\frac{\Delta z}{\Delta t}(\theta_P - \theta_P^0) = \left. \begin{array}{l} \frac{[(k(w)+P_2 D_v(\theta)g'(\theta))]_e}{\Delta z}(\theta_E - \theta_P) \\[2mm] -[\frac{k_d}{\Delta z}(\theta_P - \theta_w) + \frac{(P_2 D_v)_w}{\Delta z}(\rho_P - \rho_W)]. \end{array} \right\} \tag{6.53}$$

In the above discretized equation, the vapor densities in grid P and W are unknown at the present time step. As a numerical approximation, the values at the previous time step are used instead. Thus the vapor density term is treated as a source term, and an iterative procedure is performed to minimize the error.

The vapor density is calculated directly from the Clausius- Clapeyron equation (6.18) in the wet region, and is computed from the vapor diffusion equation in the dry region.

The condensation rate in the wet region can be computed explicitly from the vapor diffusion equation or from energy equation. The vapor diffusion equation was used to calculate the condensation rate,
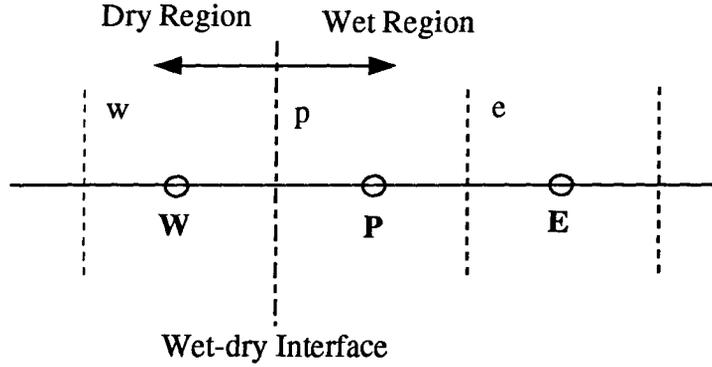
Figure 6.2: Grid-point Cluster for the Interface Location of Wet-dry Regions

$$G_P^* = \frac{D_v}{\Delta z^2} \Big|_e (\rho_{v,E} - \rho_{v,P}) - \frac{D_v}{(\Delta z)^2} \Big|_w (\rho_{v,P} - \rho_{v,W}) - \frac{(\epsilon_\gamma \rho_v)_P - (\epsilon_\gamma \rho_v)_P^0}{\Delta t}. \qquad (6.54)$$

The following boundary conditions are used for solving the condensation rate:

at the wet-dry interface, $z = z_d$,

$$G_P^* = 0, \qquad (6.55)$$

at the cold plate, $z = 1$,

$$G_P^* = \frac{2 D_v \mid e}{\Delta z^2}(\rho_{v,P} - \rho_{v,W}), \qquad (6.56)$$

which indicates that all vapor which reaches the cold plate will condense there.

The liquid fraction is computed from

$$\epsilon_{\beta,P} = \frac{G_P^*}{P_1} + \epsilon_{\beta,P}^0. \qquad (6.57)$$

Once the gas phase volumetric fraction ϵ_γ is obtained from Eq.(6.5), a source term $P_2 g(\theta) \frac{\epsilon_{\gamma,P} - \epsilon_{\gamma,P}^0}{\Delta t}$ is added to the right hand side of Equation (6.52), and the discretized energy equation for the second iteration becomes

$$[\rho c_p + P_2 \epsilon_\gamma g'(\theta)]_P \frac{\Delta z}{\Delta t}(\theta_P - \theta_P^0) = \left. \begin{array}{l} \frac{[(k(w)+P_2 D_v(\theta)g'(\theta)]_e}{\Delta z}(\theta_E - \theta_P) \\[2mm] - \frac{[(k(w)+P_2 D_v(\theta)g'(\theta)]_w}{\Delta z}(\theta_P \\[2mm] - P_2 g(\theta)\frac{\epsilon_{\gamma,P} - \theta_W) - \epsilon_{\gamma,P}^0}{\Delta t}. \end{array} \right\} \quad (6.58)$$

The other variables can be obtained from the corresponding formula for the first iteration. Satisfactory results can be obtained after 4-5 time iteration.

Stage 3: Mobile Liquid Diffusion

The discretized formulations and solution procedure for solving the temperature are similar to that of stage 2. The discretized form of the liquid transport equation is

$$\frac{\Delta z}{\Delta t}(\epsilon_{\beta,P} - \epsilon_{\beta,P}^0) = \frac{D_l \mid_e}{\Delta z}(\epsilon_{\beta,E} - \epsilon_{\beta,P}) - \frac{D_l \mid_w}{\Delta z}(\epsilon_{\beta,P} - \epsilon_{\beta,W}) + F(S) \mid_P (\epsilon_{\beta,E} - \epsilon_{\beta,P}) + \frac{G^*}{P_1}\Delta z.$$
$$(6.59)$$

The liquid starts to diffuse from the grid close to the cold boundary. Before the liquid front reaches the quasi-steady wet-dry boundary, no special boundary formula is needed for the liquid front.

The liquid front is traced where the liquid volumetric fraction is equal to, or larger than the critical liquid fraction $\epsilon_{\beta,cr.} = 0.5\epsilon_0$ (taken from Cid and Crausse's experimental data). When the liquid flows out the quasi-steady wet-dry interface, the new wet-dry interface is located at the interface of two grids where the liquid fraction in one grid exceeds the critical value in the last time step. that is assuming at the i time step, the dry-wet interface is located at the interface between grids j-1 and j, and the value of liquid fraction in grid j reaches the critical value, for the i+1 time step, the new wet-dry interface will move to interface of grid j-1, and j-2. This approximation for tracing the moving boundary is reasonable as long as the grid size is taken fine enough.

At $z = 1$, the boundary condition is

$$\frac{\Delta z}{\Delta 2t}(\epsilon_{\beta,P} - \epsilon_{\beta,P}^0) = \frac{D_l \mid_w}{\Delta z}(\epsilon_{\beta,W} - \epsilon_{\beta,P}) + F(S) \mid_P (\epsilon_{\beta,P} - \epsilon_{\beta,W}) + \frac{G^*}{P_1}\frac{\Delta z}{2}. \qquad (6.60)$$

At the moving wet-dry boundary,

$$\frac{\Delta z}{\Delta 2t}(\epsilon_{\beta,P} - \epsilon_{\beta,P}^0) = \frac{D_l \mid_e}{\Delta z}(\epsilon_{\beta,E} - \epsilon_{\beta,P}) + F(S) \mid_P (\epsilon_{\beta,P} - \epsilon_{\beta,W}) + \frac{G^*}{P_1}\frac{\Delta z}{2}. \qquad (6.61)$$

Stage 4: Long Term Liquid Accumulation and Diffusion

In this stage, the wet-dry interface reaches the exposed surface. The entire insulation slab is wet. The solution procedure for temperature is the same as mentioned for the wet region. The discretized equations (6.54) and (6.58) for the wet region are applicable for the internal grids. The boundary condition on the exposed surface is introduced as

$$\left[\rho c_p + P_2 \epsilon_\gamma g'(\theta)\right] \mid_P \frac{\Delta z}{\Delta 2t}(\theta_P - \theta_P^0) = \left.\begin{array}{l} \frac{[(k(w)+P_2 D_v(\theta)g'(\theta))]\mid_e}{\Delta z}(\theta_E - \theta_P) \\[2mm] -h_a(\theta_P - \theta_a) - P_2 h_m(\rho_P - \rho_a)]. \end{array}\right\} \qquad (6.62)$$

Similar boundary conditions on the exposed surface are also introduced for computing the condensation rate and liquid fraction.

6.3.2 The Solution Algorithm

A Fortran 77 computer code has been developed to solve the above-stated system of the coupled nonlinear equations. Starting with the initial values of the temperature and vapor density, the solutions of the above model for the four stages involve several formats, as well as several iteration procedures. These formats are:

- Format 1. This format was followed for any time and location along slab for which no condensation occurs in the insulation slab.

  1. Initial values of θ and ρ_v are given from Equation (6.13), (step 1 is applied only at $t = 0$).

  2. The condensation rate is set to zero, θ is obtained from Equation (6.20) and ρ_v is obtained from Equation(6.19).

  3. The saturated vapor density $\rho_{v,s}$ is obtained from Eq. (6.18) based on the computed temperature profile.

  4. If, at any location, the ρ_v obtained in step 2 is greater than or equal to $\rho_{v,s}$ obtained from step 3, then Format 2 is adopted for the next time step. Otherwise the procedure starting from step 2 is repeated for the next time step.

- Format 2. This format was followed for any time and location for which the wet region is established and $\epsilon_\beta < \epsilon_{\beta,cr}$.

  1. The temperature in the wet region is solved from Equation (6.52) with boundary conditions (6.53) and (6.16) as the first iteration.

  2. The vapor density in the wet region is obtained from Equation (6.18).

  3. The temperature and vapor density in the dry region are obtained from Equation (6.20) and (6.19).

  4. The condensation rate is obtained from Equations (6.54) -(6.56).

  5. The liquid phase fraction ϵ_β is obtained from Equation (6.57), and the gas phase fraction ϵ_γ is obtained from the volumetric constraint Equation (6.5).

  6. The second iteration value of the temperature in the wet region is obtained from Equation (6.58).

7. The same procedures are followed from step 2 to step 5 to obtain the second iteration values of vapor density, condensation rate and the liquid fraction.

8. If, at any location, the liquid fraction obtained from step 7 is greater than or equal to the critical liquid fraction, Format 3 is adopted for the next time step. Otherwise, the procedure starting from step 1 is repeated for the next time step.

- Format 3. This format was followed for any time and location for which the liquid volumetric fraction exceeds the critical liquid volumetric fraction.

1. The temperature field in the wet region is solved from Equation (6.52) with boundary conditions (6.53) and (6.16) as the first iteration.

2. The vapor density in the wet region is obtained from Equation (6.18).

3. The temperature and vapor density in the dry region are obtained from Equation (6.20) and (6.19).

4. The condensation rate is obtained from Equations (6.54) -(6.56).

5. The liquid phase fraction ϵ_β is obtained from Equation (6.59), with the boundary conditions (6.60), (6.61). The gas phase fraction ϵ_γ is obtained from the volumetric constraint Equation (6.5).

6. The second iteration value of the temperature in the wet region is obtained from Equation (6.58).

7. The same procedures are followed from step 2 to step 5 to obtained the second iteration values of vapor density, condensation rate and the liquid fraction.

8. If $z_d=0$, Format 4 is adopted for the next time step. Otherwise, the procedure starting from step 1 is repeated for the next time step.

- Format 4 This format was followed for any time and location for which all the locations are wet.

1. The first iteration value of temperature is obtained from Equation (6.52) with boundary conditions (6.16) and (6.6.62).

2. The vapor density in the wet region is obtained from Equation (6.18).

4. The condensation rate is obtained from Equations (6.54),(6.56) and (6.63).

5. The liquid phase fraction ϵ_β is obtained from Equation (6.59), with the boundary conditions (6.60), (6.61). The gas phase fraction ϵ_γ is obtained from the volumetric constraint Equation (6.5).

6. The second iteration value of the temperature in the wet region is obtained from Equation (6.58).

7. The same procedures are followed from step 2 to step 5 to obtained the second iteration values of vapor density, condensation rate and the liquid fraction.

The discretization equations for the above one-dimensional formulation can be solved by a delightly convenient algorithm, called TriDiagonal -Matrix Algorithm (TDMA). In principle, all the above-mentioned formulations have a form similar to the equation system (6.41)-(6.46). The nonzero coefficient of the set of equations defined by Equation (6.41) form a tri-diagonal matrix. The convergence of TDMA is fast because the boundary condition information is transmitted at once to the nodal points lying inside the solution domain.

It should be pointed out that although there are two groups of formulation for the wet and dry regions respectively in the stage 2 and 3, these two groups of discretization equations should be solved in one matrix. Numerical errors may occur when the solutions of field variables are attempted separately from the dry and wet regions. There are two

reasons for this. First, the dry region is being reduced due to the moving interface, and the TDMA will lose effectiveness when the dimension of the matrix is less than 3. The second reason is that nodal points inside the solution domain are blind to the information of another domain.

6.4 Numerical Considerations

- Grid System and Time Step

  Two checks were made in order to investigate the accuracy of the scheme. First, the three different grid systems, given by 50, 100 and 150 grids, were used to test the effects of the grid size on heat transfer rate, the wet-dry interface location, and the distributions of the field variables. It was found that an excellent agreement exists between the results from 100 and 150 grid systems. Next, the time step size was checked by fixing the grid size with 100 grids while varying the time step size as 30s, 60s, 120s, 180s, 240s, 360s etc.. As the results show, decreasing the time step size beyond 180 seconds did not have an effect on the numerical results.

  The accuracy of the wet-dry interface position depends on the selection of the grid size. For this reason, the grid size should be chosen as fine as possible. However, the required time step size becomes much smaller as the grid is refined. Considering the balance between accuracy and economy of computing time, a grid system with 100 grids and a time step of 120 seconds were chosen for the numerical computation.

- Iterative Scheme

  In computing the field variables such as temperature θ in the wet region, several iteration schemes were needed. In order to handle nonlinearities in the iteration solutions of the discretization equations, it was necessary to underrelax the iteration

process. The solution was considered to be converged when the deviation of any variable from the last iterated value was within 0.01%.

- Numerical Errors and Instabilities

Numerical errors and instabilities can be caused by inappropriate numerical parameters such as coarse grids, too large a time step and underrelaxation factors, as well as unrealistic initial values. The correct evaluation of numerical parameters can be achieved from the numerical experiments.

Chapter 7

NUMERICAL RESULTS AND DISCUSSIONS

7.1 Introduction

The numerical model presented in the previous Chapter was used to investigate transient heat and mass transport accounting for phase change in a fibrous insulation slab. One of the main objectives of this work was to simulate the thermal behavior of porous insulation including dynamic response during the diffusion and condensation process. The numerical formulation and its solution methodology are validated by the comparison of numerical results with the experimental data of Wijeysundera et al.. The variation and intercoupling effects of important field variables such as temperature, vapor density, condensation rate and liquid fraction are presented. Heat transfer rate through the insulation is quantified, and the moisture accumulation and distribution are numerically simulated. The long term effects of the moisture transport on thermal performance of the insulation were studied, and the interesting effects of variation of physical characteristics on the moisture and energy transfer are discussed.

7.2 Physical Data

In order to examine the validity of the numerical model, the physical data used in the numerical computation are based on the fibrous insulation which was tested as an experimental sample, and also based on the real experimental conditions [23]-[25]. The physical data are summarized in Table 7.1.

ρ_0^*	53 kg/m^3	ρ_β^*	999.87 kg/m^3
$c_{p,0}^*$	840 J/kg K	$c_{p,\beta}^*$	4200 J/kg K
k_0^*	0.037 W/m K	k_β^*	0.57 W/m K
$\alpha_{0,eff}^*$	8.84(10)$^{-7}$ m^2/s	ρ_a^*	1.15 kg/m^3
ρ_σ^*	2600 kg/m^3	$c_{p,a}^*$	1005 J/kg K
$c_{p,\sigma}^*$	836.8 J/kg K	k_a^*	0.57 W/m K
k_σ^*	0.762 W/m K	$c_{p,v}^*$	1882 J/kg K
ϵ_σ	0.02	$p_{v,0}^*$	2337 bar
R_v	461.89 J/kg K	h_{fg}	2450000 J/kg

Table 7.1: Physical Data.

7.3 Diffusion and Condensation Processes

7.3.1 Initial Process

The dynamic response of porous insulation subjected to the specified boundary conditions has been investigated by case studies. Figures 7.1-7.4 illustrate the distribution of the temperature, vapor density, condensation rate, and liquid fraction in the initial stage. As can be seen in Figure 7.1, when a porous insulation slab is suddenly exposed to the ambient air on one side, and is subjected to a temperature drop on the other side, this temperature drop propagates from the cold side into the insulation slab with time. Under the given boundary conditions, the temperature field becomes quasi-steady after about half an hour (2040 seconds). The propagating behavior is also observed for vapor density as shown in Fig. 7.2, and the vapor density field reaches the quasi-steady state after about the same period. It is apparent that the drop of vapor density propagates faster than that of temperature. It can be expected as the Lewis number which is a measure of the relative importance of heat transport to the vapor transport, is less than one.

The distribution of condensation rate with time is shown in Fig. 7.3. The condensation occurs first at the cold plate, and then takes place within the insulation slab after
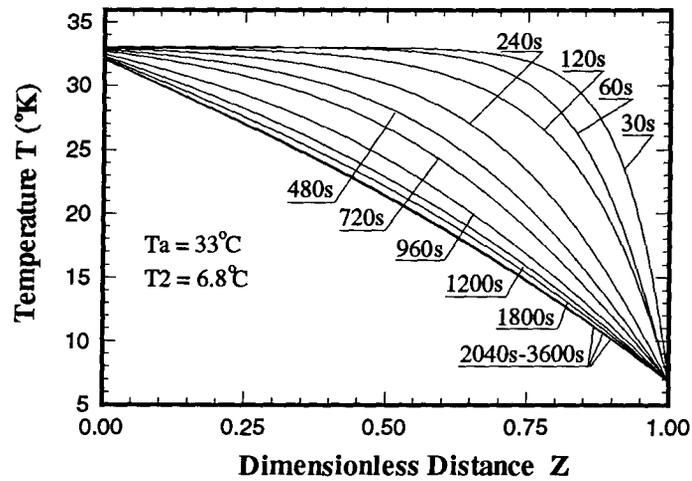
Figure 7.1: Temperature Distribution in the Initial Stage; $\rho^* = 53$ kg/m^3, $L = 66$ mm, $RH = 96\%$, $h^* = 12$ W/m^2 K.
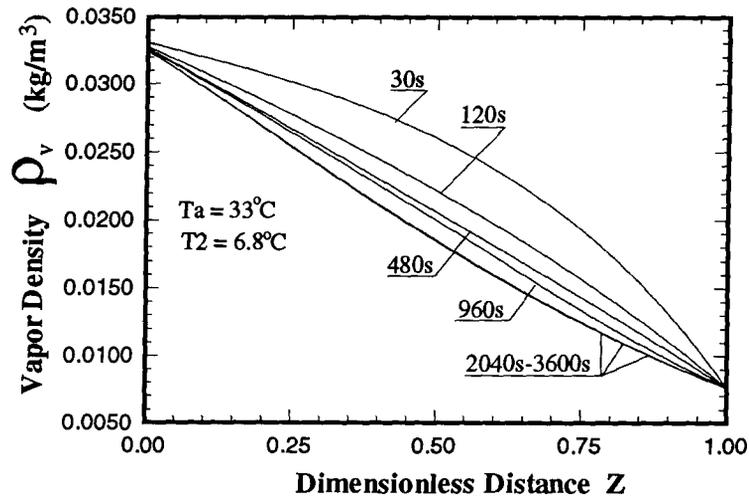
Figure 7.2: The Distribution of Vapor Density in the Initial Stage; $\rho^* = 53$ kg/m^3, $L = 66$ mm, $RH = 96\%$, $h^* = 12$ W/m^2 K.
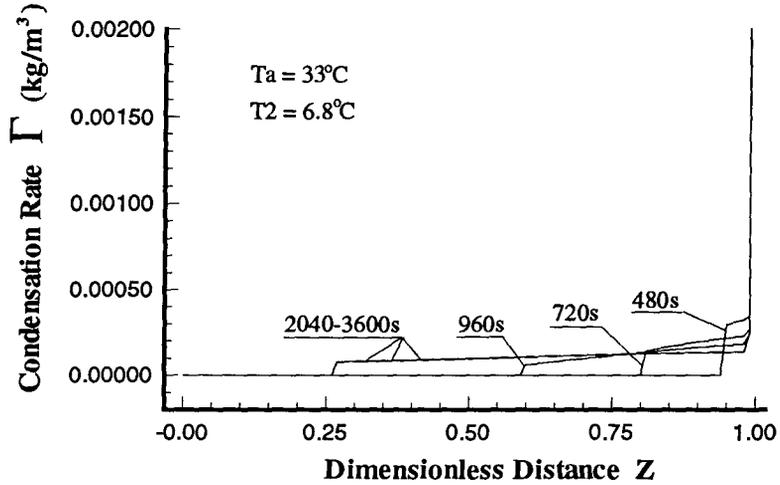
Figure 7.3: The Time Variation of Condensation Rate in the Initial Stage; $\rho^* = 53$ kg/m^3, $L = 66$ mm, $RH = 96\%$, $h^* = 12$ W/m^2 K.
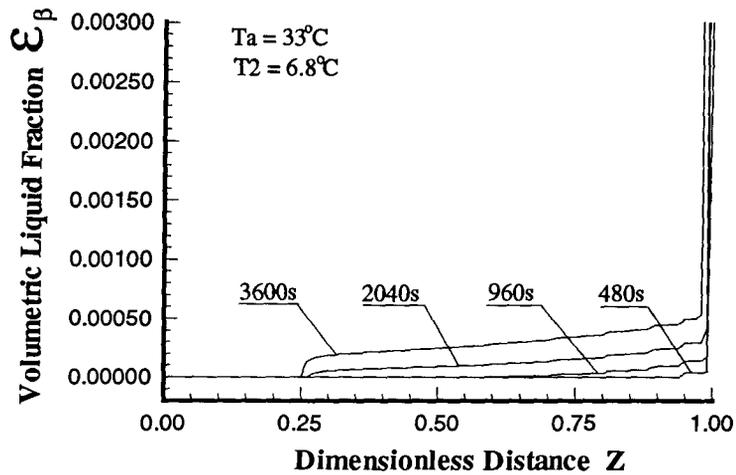

Figure 7.4: The Time Variation of Volumetric Liquid Fraction in the Initial Stage; $\rho^* = 53$ kg/m^3, $L = 66$ mm, $RH = 96\%$, $h^* = 12$ W/m^2 K.

about 480 seconds. The condensation occurs within the slab when the local saturation density is decreased below the actual vapor density. With the propagation of temperature drop in the slab, the location of the condensation front moves towards the warmer side, and stops at some place when the temperature field becomes quasi-steady. The condensation rate is highest at the cold plate because all the vapor flux is condensed there. The liquid fraction is accumulated with time due to condensation as shown in Fig. 7.4. In the initial stage, it attains its highest value at the cold plate.

7.3.2 Quasi-steady State Period

Figures 7.1 and 7.2 show that after a period of time the distributions of temperature and vapor density remain constant. Fig. 7.3 shows that after about the same period, the location of the condensation front is fixed at some place which indicates the quasi-steady wet-dry interface. The quasi-steady behavior of temperature and vapor density with respect to time indicates reduction of transient thermal, mass and diffusion processes. The liquid fraction ϵ_β still increases with time due to a constant condensation rate.

For the illustrative case shown in Figs. 7.1-7.4, the quasi-steady state is reached in 2040 seconds. Fig. 7.5 shows the temperature distributions along the insulation slab after a quasi-steady state has been established; the numerical results are compared with the analytical results in Chapter Five. The experimental results under the same conditions are also plotted in Fig. 7.5, which shows good agreement.

7.3.3 Liquid Accumulation and Diffusion

The profiles of liquid volumetric fraction over a period of 120 hours are shown in Figure 7.6. Initially, vapor condensation occurs mainly on the cold surface. The liquid generated is accumulated at the impermeable cold plate and the nearby insulation layer. With the establishment of a quasi-steady state, liquid is accumulated in the wet region at a constant
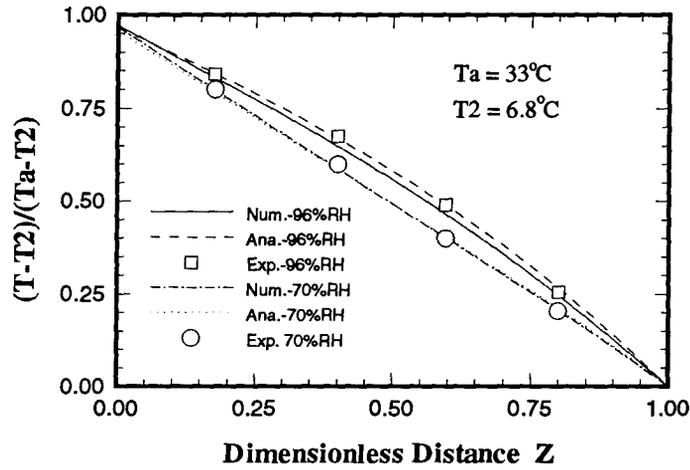
Figure 7.5: Temperature Distribution in the Quasi-steady State Period, Comparison of Numerical, Analytical and Experimental Results [22]; $\rho^* = 53$ kg/m^3, $L = 66$ mm, $RH = 96\%$, $h^* = 12$ W/m^2 K.
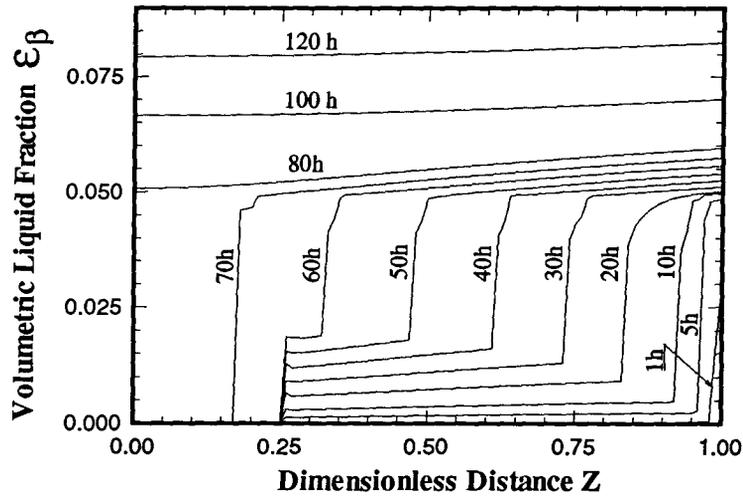

Figure 7.6: The Time Variation of Liquid Fraction over a Long Term Period; $\rho^* = 53$ kg/m^3, $L = 66$ mm, $RH = 96\%$, $h^* = 12$ W/m^2 K, $T_a = 33^{\circ}C$, $T_2 = 6.8^{\circ}C$.

rate. The curve at 1 hour indicates that the liquid fraction at the impermeable cold boundary is higher than the critical value, and the liquid diffuses from the cold surface into the insulation slab. From the curves from 5 hours to 60 hours, we can see clearly that the liquid diffusion front moves towards the dry side. Before the liquid diffusion front arrives, the liquid fraction accumulates slowly with time. It increases sharply when the liquid diffusion front arrives. The liquid front can flow out the quasi-steady boundary as indicated by the curve at 70 hours, and eventually reaches the exposed surface, as shown by the curves from 80 hours to 120 hours. In the later stage, the liquid fraction is higher than the critical value in the entire insulation slab. The liquid diffuses from one layer into the adjoining layer with the resultant increase in liquid content and a corresponding leveling of the liquid content in the upstream layers. In addition to this transport mechanism, the local liquid content still increases due to the local condensation. Since the liquid amount produced by condensation is still highest on the impermeable cold plate, the liquid will diffuse under the liquid fraction gradient, i.e. from the impermeable surface towards the exposed surface.

7.4 Comparison with Experimental Results

Wijeysundera et al. [23, 24, 25]] had measured the temperature distribution, heat flux, total moisture gain, and the liquid distribution for a range of experimental conditions through five runs. The testing times ranged form 300 to 600 hours. In the present work, case studies have been performed by comparing the computational results with the experimental data. The comparisons of the temperature distributions, heat transfer rates at the impermeable plate, the total moisture gain and liquid distribution with the experimental data are presented respectively in the following sections.

7.4.1 Temperature and Heat Transfer

Sixty six cases of measured temperature distribution tn different times for five operating conditions have been simulated. For brevity, only the comparisons with the experimental data for 16 cases are presented in Figs. 7.7 - 7.10. There is very good agreement between the measured and computed temperature distributions. It should be pointed out that the uncertainty of the thermocouples location in the insulation slab may be responsible for some fluctuations in the measured data.

The comparisons of computed and measured heat flux at the impermeable cold plate for four runs are shown in Fig. 7.11. The computed heat flux at the cold plate is summed up from two components. The first component is conductive heat flux which depends on the thermal conductivity of the moisture laden insulation; so called 'solid thermal conductivity'. The second is latent heat due to the condensation of the vapor reached the cold plate. Fig. 7.11 shows that the numerical model underpredicts the heat flux at the cold plate. The reason for the discrepancy may be due to the accuracy of moisture laden thermal conductivity models. Several possible thermal conductivity models are listed in Appendix B. Among these, the bead arrangement model is chosen for representative computation after a comparison of these models which will be discussed later. The fluctuations in the heat flux curves are due to the nonuniform temperature difference between the ambient air and the cold plate in the experiments.

7.4.2 The Moisture Gain and Liquid Transport

The total moisture gain per unit volume of the slab is obtained by integrating numerically the liquid content over all the finite control volumes. The comparison of computed total moisture gain with measured data under four different operating conditions is shown in Fig. 7.12. The numerical results show good agreement with measurements for the first
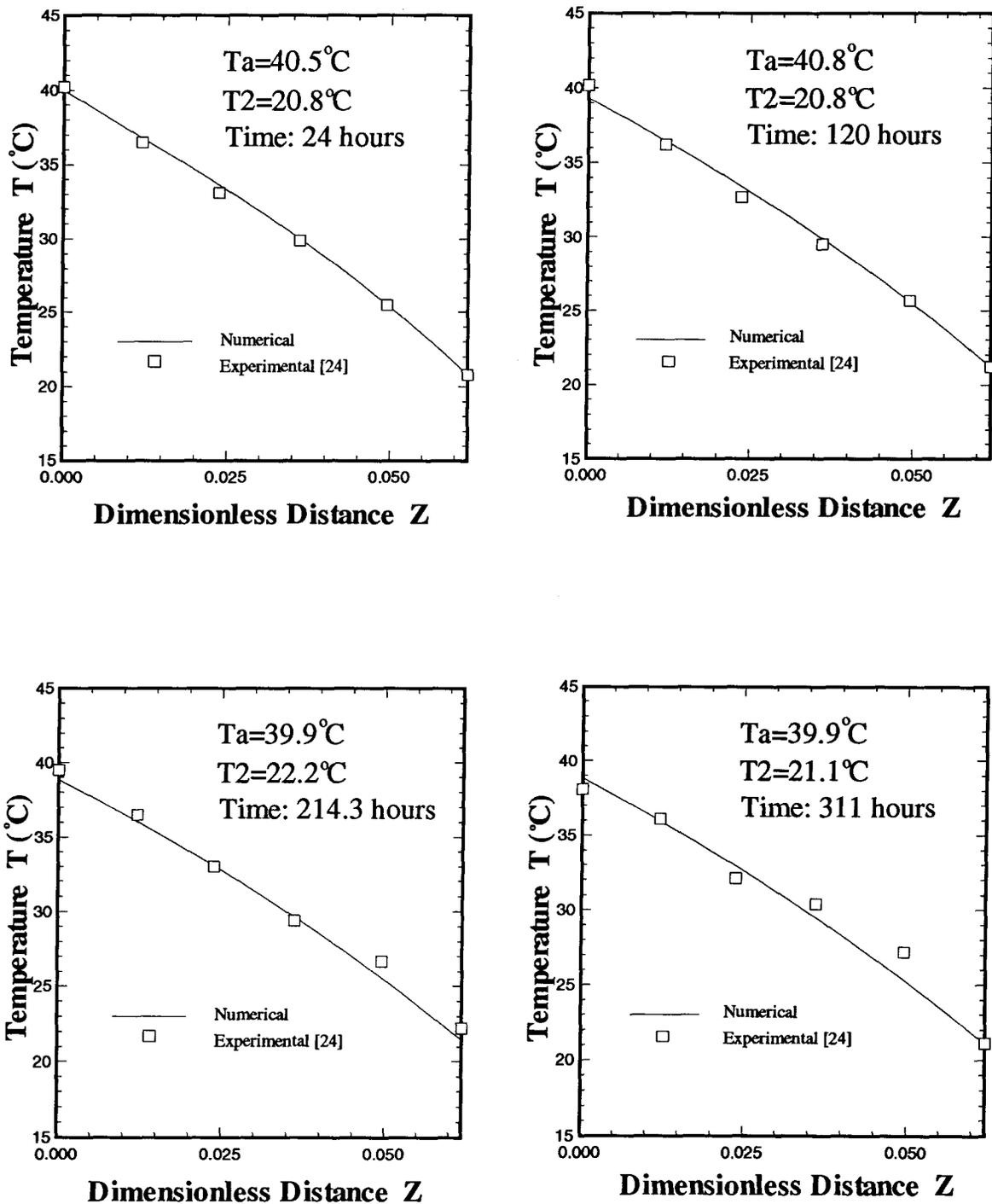
Figure 7.7: The Temperature Distributions in Run 1, Comparison of Numerical Results with Experiment Data [24]; $\rho^* = 53$ kg/m^3, $L = 62.02$ mm, $RH = 97\%$, $h^* = 12$ W/m^2 K.
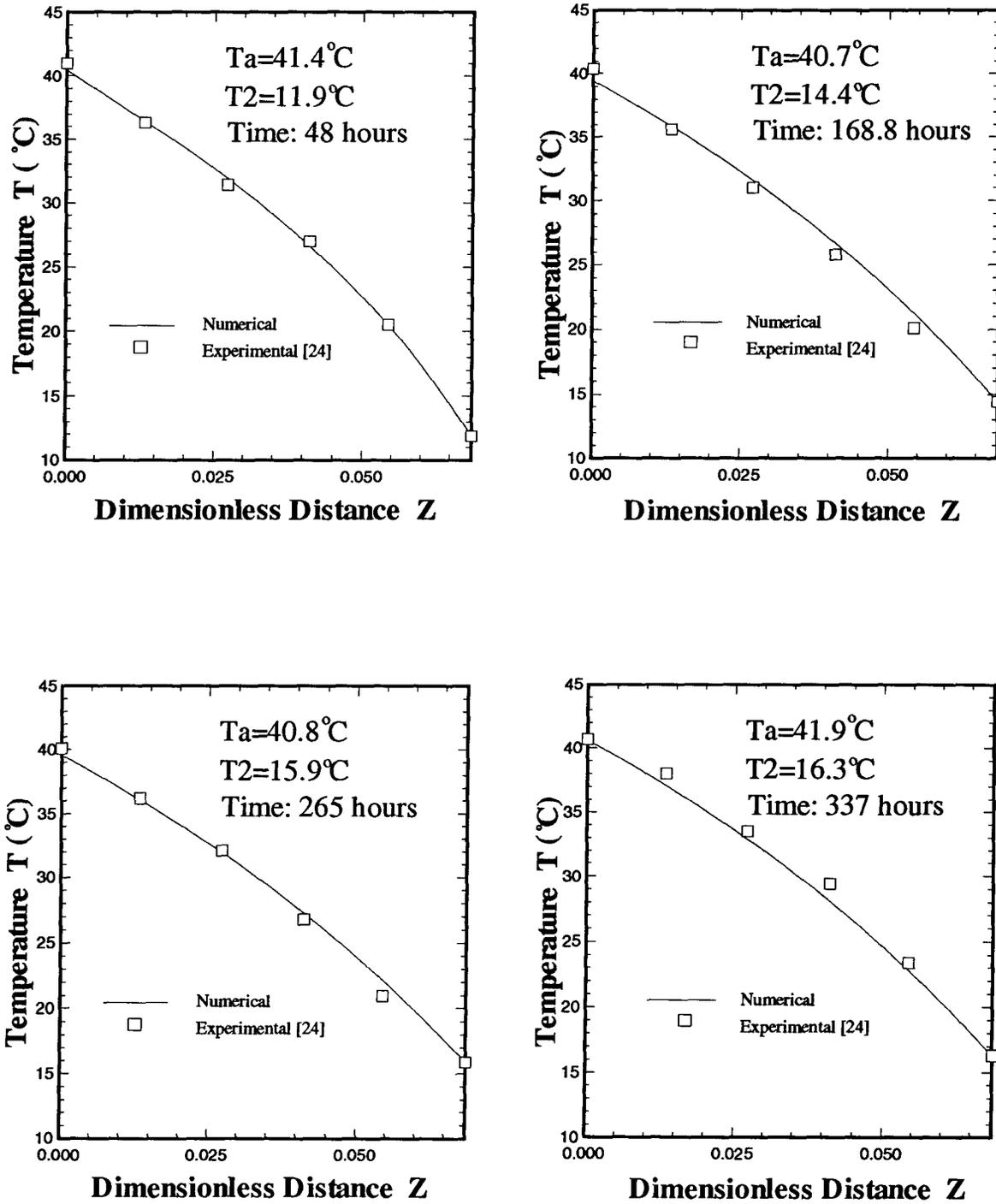
Figure 7.8: The Temperature Distributions in Run 2, Comparison of Numerical Results with Experiment Data [24]; $\rho^* = 53$ kg/m^3, $L = 68.65$ mm, $RH = 96.5\%$, $h^* = 12$ W/m^2 K.
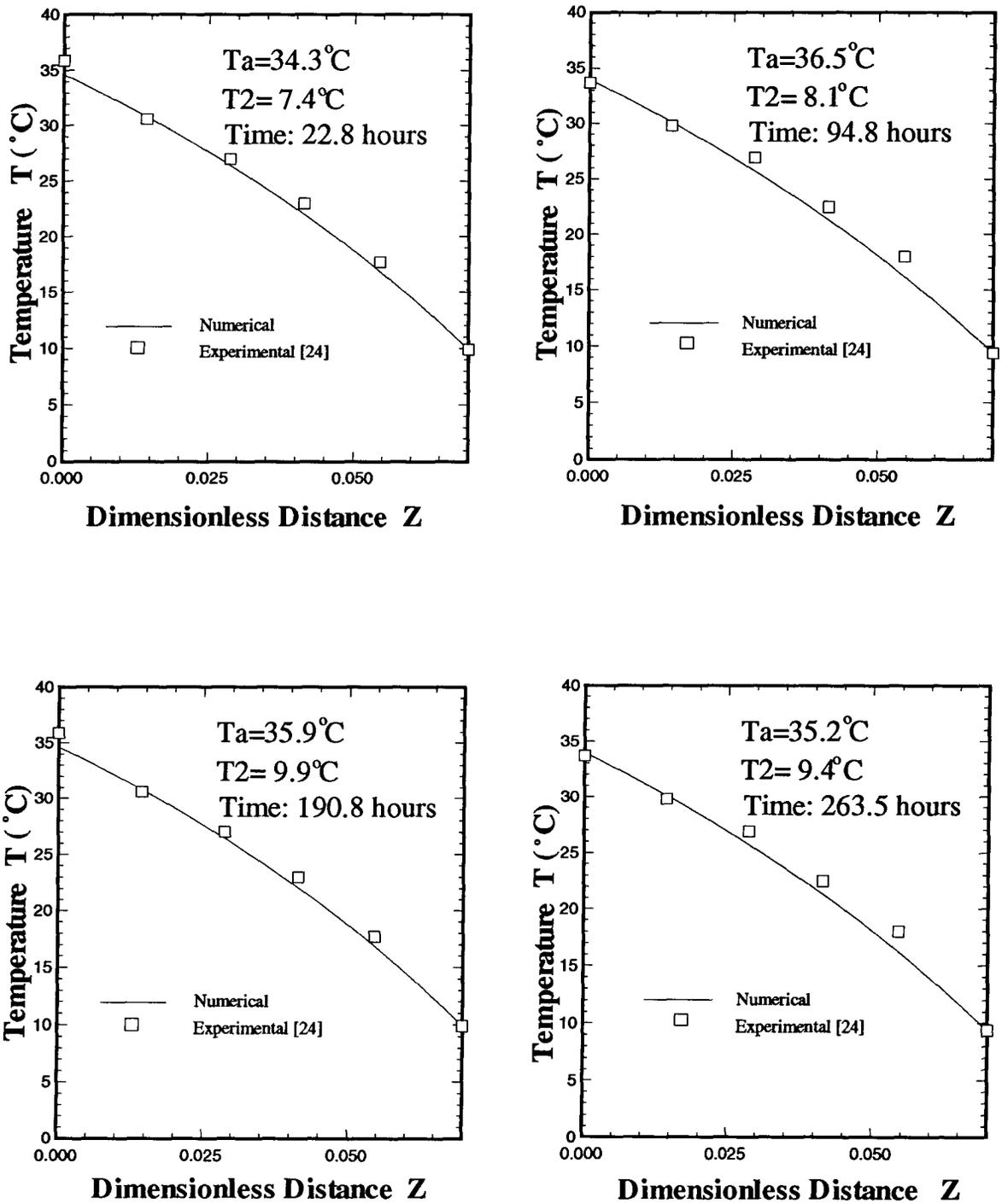
Figure 7.9: The Temperature Distributions in Run 3, Comparison of Numerical Results with Experiment Data [24]; $\rho^* = 53$ kg/m^3, $L = 70$ mm, $RH = 96\%$, $h^* = 12$ W/m^2 K.
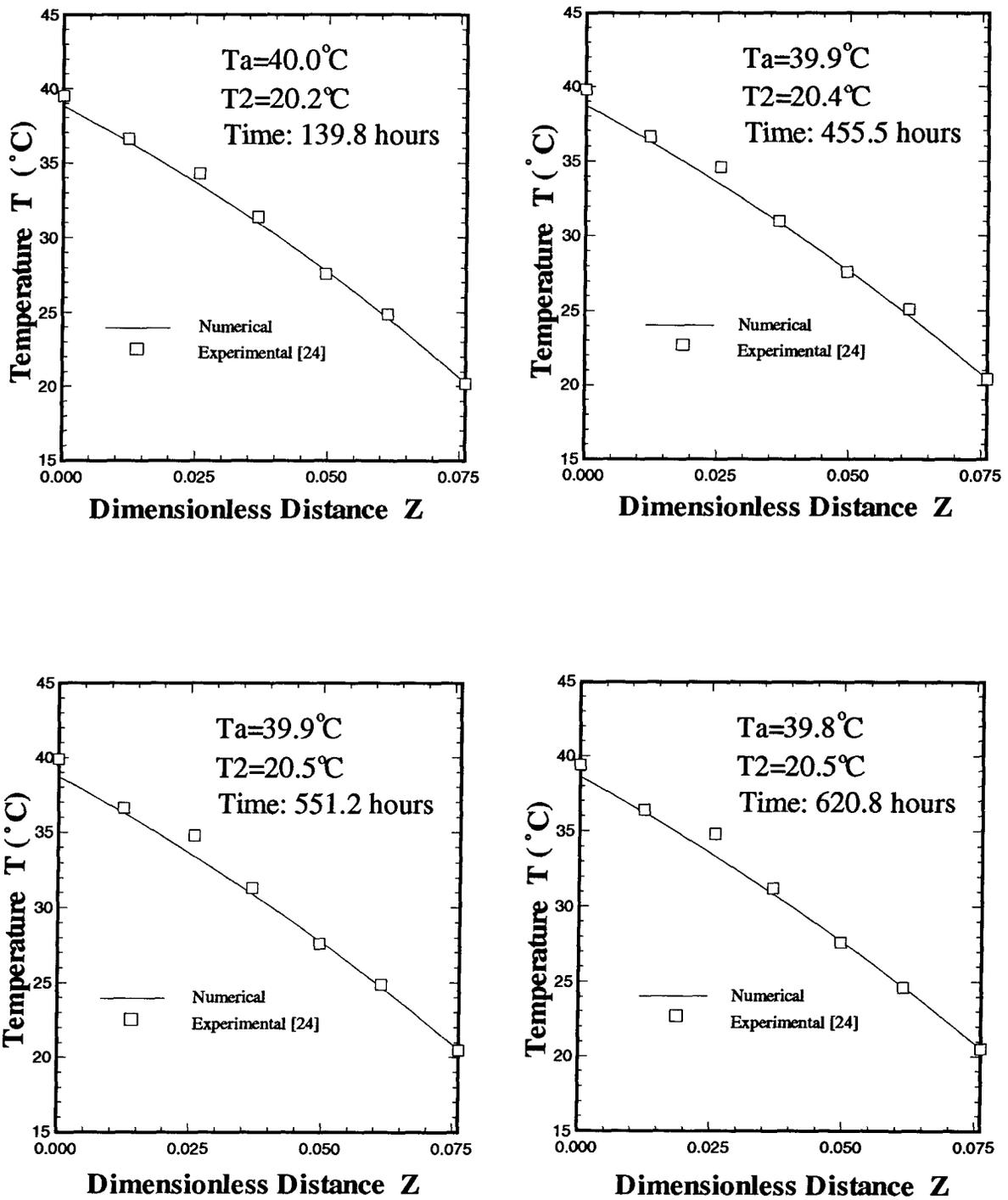
Figure 7.10: The Temperature Distributions in Run 5, Comparison of Numerical Results with Experiment Data [24]; $\rho^* = 53$ kg/m^3, $L = 76.13$ mm, $RH = 96\%$, $h^* = 12$ W/m^2 K.
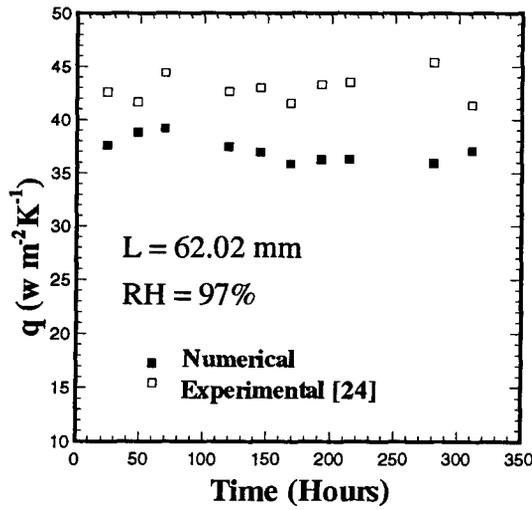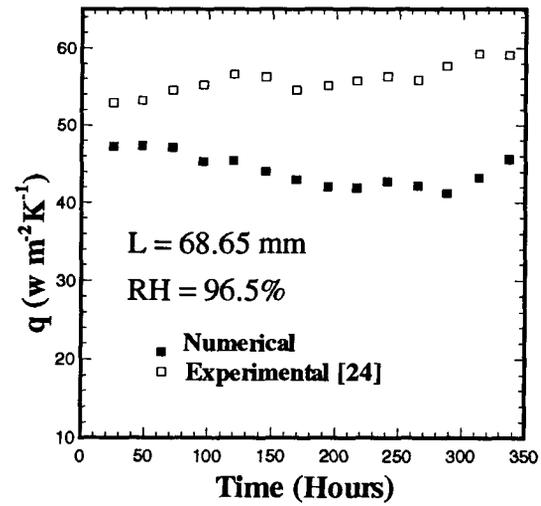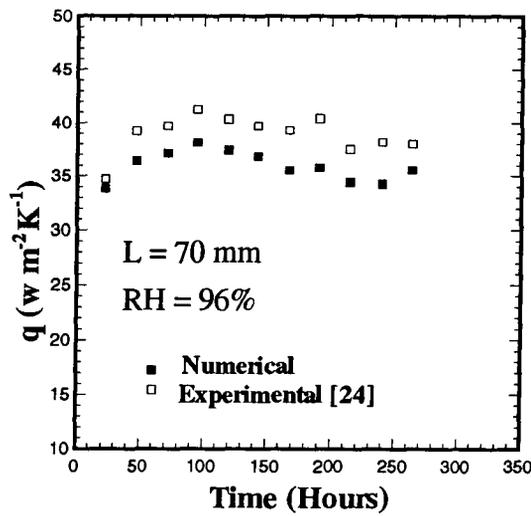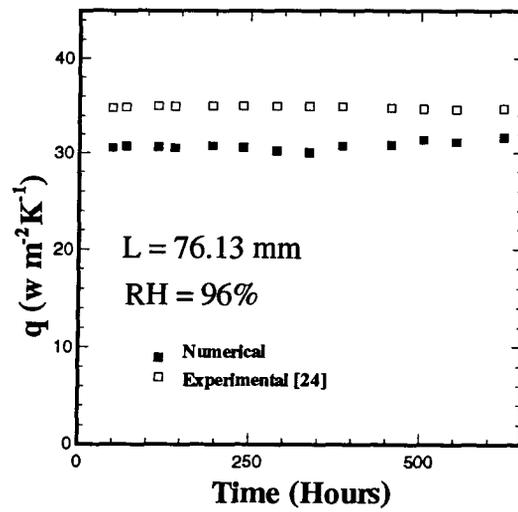
Figure 7.11: The Heat Flux at the Cold Plate, Comparison of Numerical Results with Experiment Data for Four Runs [24]; $\rho^* = 53$ kg/m^3, $h^* = 12$ W/m^2 K.

three runs, especially for run 3 shown in Fig. 7.12(c). Fig. 7.12(d) shows that in the longer times, the predicted total moisture gain is higher than the measured data. This may be due to the decrease in vapor diffusion coefficient with liquid concentration which has not been taken into account in this model.

The measured spatial distribution of the average liquid concentration was obtained by measuring the increase in mass of the different insulation layers. The comparison of the computed and measured spatial distribution of the average liquid concentration is shown in Fig. 7.13 for run 1. Fig. 13 (a) shows good agreement between the computed results with the measured data for a period up to 70 hours. The liquid distributions in this period display similar trends. The liquid produced by condensation is deposited mostly in the insulation layer adjacent to the cold plate, and is forced towards the next layer with time. Fig. 13(b) shows the comparison of computed results with experimental data at 120 and 144.5 hours respectively. Two apparent discrepancies can be observed from this plot. First the predicted liquid movement is faster than the measured. In the measurement, the liquid is trapped in the layer adjacent to the cold plate untill the layer attains a very high liquid content. This indicates that the liquid diffusivity becomes significant only when liquid fraction reaches a very high value (approximately $\epsilon_\beta > 0.2$ for this case). This phenomenon did not appear in Cid and Crausse's experimental work [28]. The second discrepancy is on the average liquid concentration of the layer with the exposed surface. The experimental data shows a rapid rise of average liquid concentration of that layer after a certain period while the numerical model predicts a far slower growth of average liquid concentration in the layer. The present model can not explain why the layer with the exposed surface has higher liquid content than in the inner layers. A physical explanation for this behavior given by Wijeysundera et al. [25] is the tendency for the layer with the exposed surface to accumulate liquid due to the surface tension forces between water and the last layer of fibers on the exposed

(a) Run 1

(b) Run 2

(c) Run 3

(d) Run 5
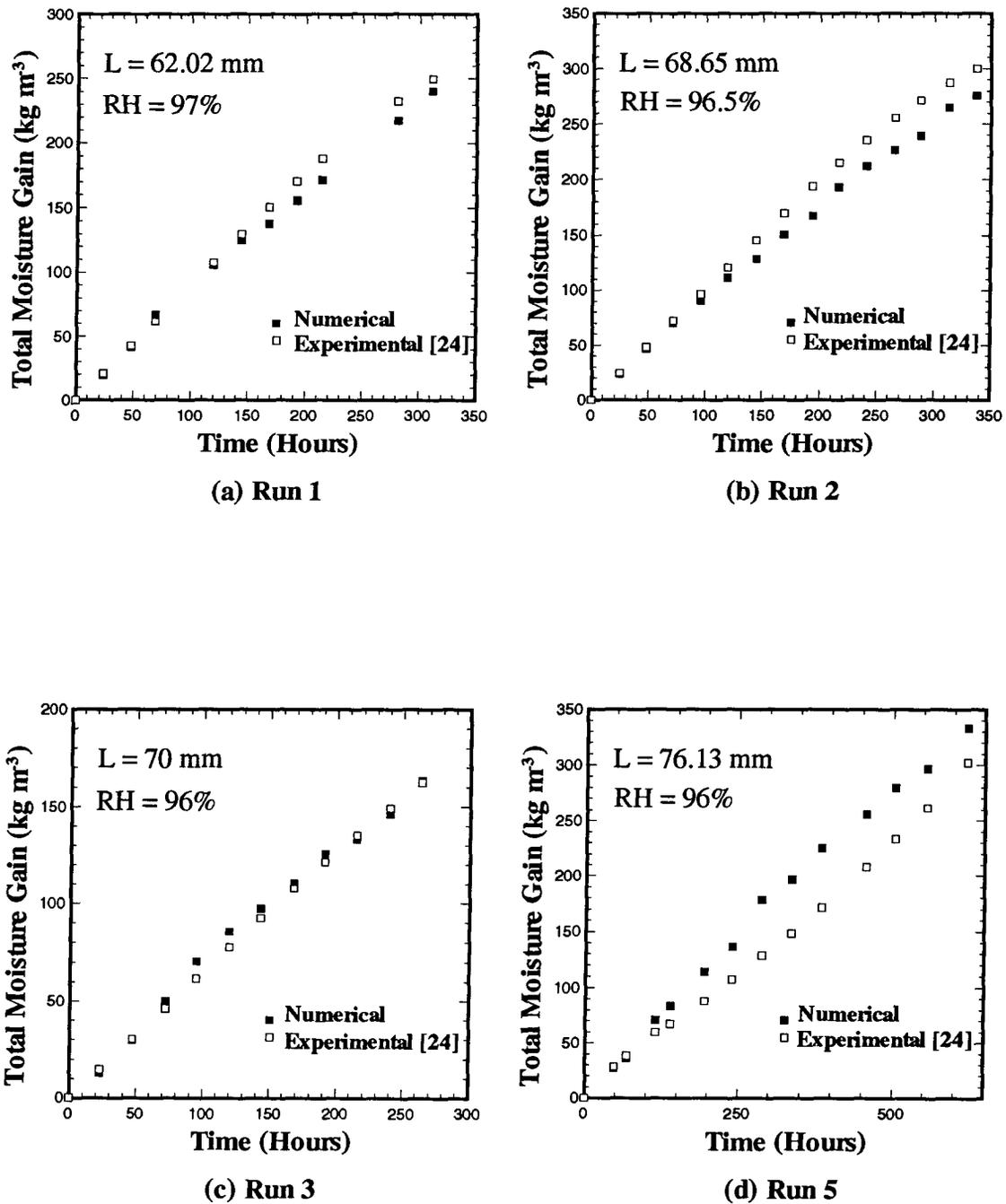
Figure 7.12: The Total Moisture Gain, Comparison of Numerical Results with Experiment Data for Four Runs [24]; $\rho^* = 53$ kg/m^3, $h^* = 12$ W/m^2 K.
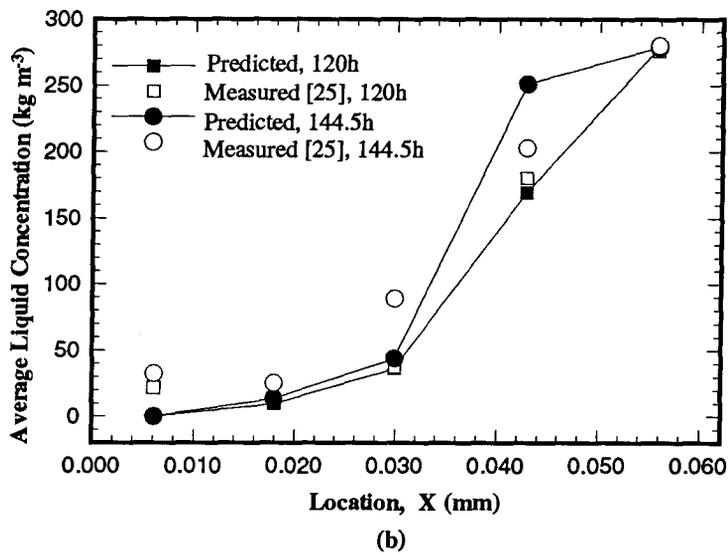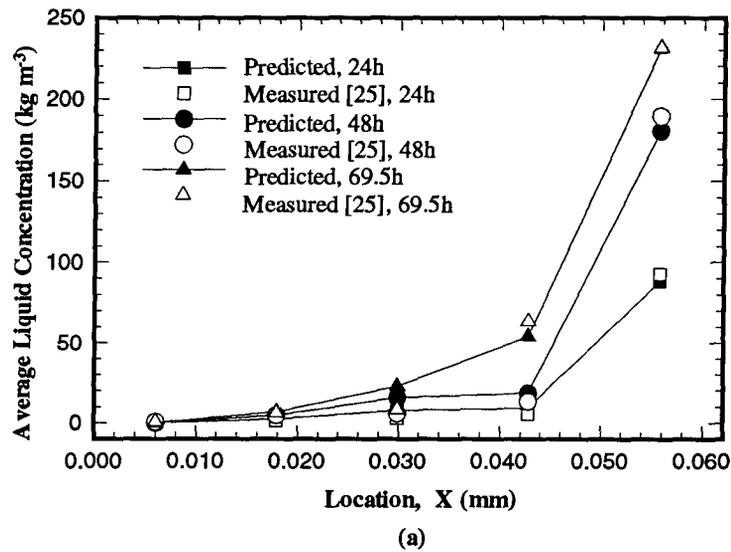
Figure 7.13: The Liquid Distribution in Slab at Different Times, Comparison of Numerical Results with Experiment Data [24]; Run 1. $\rho^* = 53$ kg/m^3, $h^* = 12$ W/m^2 K, $L = 62.02$ mm.

surface. However, the reason for liquid penetrating the inner layers without becoming trapped there is unknown. The effect of gravity may be an explanation for this. Since the mechanism of moisture movement and the liquid path through the fibers in fibrous insulation are not known, theoretical simulation of liquid transport process in fibrous materials requires a more rigorous model of liquid transport coefficients.

7.5 Thermal and Transport Performances

7.5.1 The Variation of Heat Flux

The variation of heat flux at cold boundary with time under fixed temperature difference between the ambient and cold plate, as well as the variation of the two components which contribute to the total heat flux, are shown in Fig. 7.14. The conductive component shows an increasing trend with times because of the increasing 'solid' thermal conductivity (which is a result of increased liquid content). The latent heat component decreases with time due to the reduction of vapor flux from ambient. However, the total heat flux shows an increasing trend with time, which suggests that the apparent thermal conductivity due to laden moisture has been increased adequately to bring this about.

A dramatic increase in heat flux occurs when the liquid flows out the wet-dry interface. It attains its peak value when liquid front reaches the exposed surface, then decreases to normal values and rates. This phenomenon is complicated by the combination of evaporation and condensation which occur when liquid enters an unsaturated region. Liquid flows into the dry region forced by capillary action. When liquid encounters the warmer, unsaturated water vapor-air mixture, evaporation will occur at the liquid front. Some vapor is produced in the local space. Since the liquid amount which is forced from high liquid content region to the dry region is large, the result of liquid mixed with unsaturated water vapor is a saturated liquid-gas mixture which reaches a new
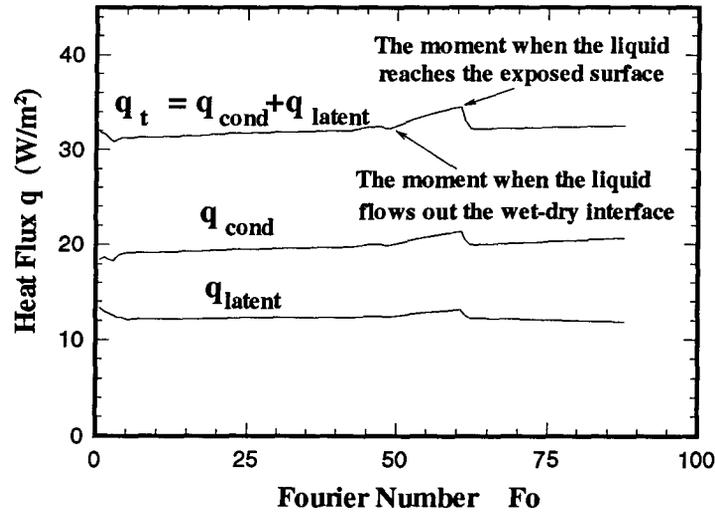
Figure 7.14: The Variation of Heat Flux at Cold Boundary with Times; $\rho^* = 53$ kg/m^3, $h^* = 12$ W/m^2 K. $T_a = 33^\circ C$. $T_2 = 6.8^\circ C$. $RH = 90\%$.
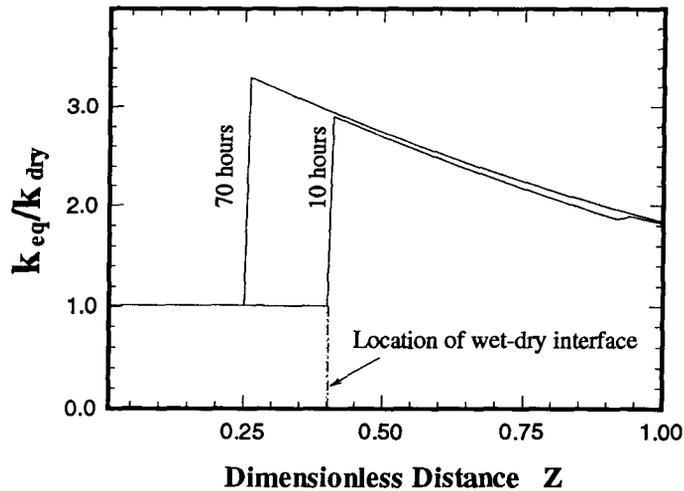
Figure 7.15: The Variation of Equivalent Thermal Conductivity along the Insulation Slab; $\rho^* = 53$ kg/m^3, $h^* = 12$ W/m^2 K, $T_a = 33^\circ C$, $T_2 = 6.8^\circ C$, $RH = 90\%$.

equilibrium state. The region which the liquid front occupies becomes saturated. The outflowing liquid empties its space in the wet region, which enables an increasing vapor flux into the insulation slab. The condensation rate and the condensation amount increase in the wet region. Subsequently, both the moisture laden conductive heat and latent heat increase. After the liquid front reaches the exposed surface, the entire insulation slab is saturated. The temperature and vapor density fields regain their quasi-steady behavior, and the condensation rate returns to a constant rate.

The equivalent thermal conductivity at any cross section is defined by the following expression:

$$q_i = -k_{eq} \frac{dT}{dx} \big|_{x_i} . \tag{7.1}$$

The ratio of equivalent thermal conductivity to the dry state thermal conductivity represents the effect of condensation on the thermal performance of insulation. The variation of equivalent thermal conductivity ratio along the slab at selected moments is shown in Fig. 7.15. As can be expected, the equivalent thermal conductivity ratio is unity in the dry region. It increases significantly in the wet region and attains a maximum value near the wet-dry interface. The curves of equivalent thermal conductivity decline gradually in the direction of the cold side due to the reduction of vapor flux in that direction.

7.5.2 Effect of Humidity Levels

The effective thermal conductivity ratio and the total moisture gain under different humidity levels in the ambient are presented in Fig. 7.16. The term k_{eff}/k_{dry} in Fig. 7.16(a) represents the ratio of conventional effective thermal conductivity at cold boundary to the dry state thermal conductivity of insulation (for brevity, all thermal conductivity

ratios which appeare in the following refer to the ratio at the cold boundary). Humidity levels on the exterior boundary have a significant influence on the heat flux and the total liquid concentration. This is because increasing the humidity level enhances the vapor transport, and the enhancement in vapor transfer will in turn cause an increase in heat transfer. It is also noted that a higher humidity level on the exterior boundary reduces the time to reach a quasi-steady state. As can be observed in Fig. 7.16(a), decreasing the humidity level reduces the quasi-steady wet region, thus reducing the time for liquid to flow out of the wet region.

7.5.3 Effect of Convective Heat Transfer Boundary Conditions

Interesting results are obtained through the examination of the effect of the ambient convective heat transfer coefficient. Fig. 7.17 shows the variations of k_{eff}/k_{dry} and the moisture gain with time. It is noted that k_{eff}/k_{dry} decreases with increasing heat transfer coefficient. Since increasing convective heat transfer at the exterior boundary enhances the temperature penetration inside the slab, and the saturation vapor density is mainly dependent on the temperature distribution, the wet region in the slab is reduced as a result. The reduction of the wet region leads to decreases of condensation rate. Subsequently, the moisture laden thermal conductivity is decreased, as well as the latent heat flux. Therefore the total heat flux through the insulation slab decreases with an increasing of ambient convective heat transfer coefficient. The above-mentioned results indicate the complex intercoupled nature of heat and mass transport in these types of problems.

7.5.4 Effect of Slab Thickness

The effects of insulation slab thickness on thermal performance and liquid accumulation in an insulation slab are shown in Fig. 7.18. As can be expected, with a decrease of slab

(a)

(b)
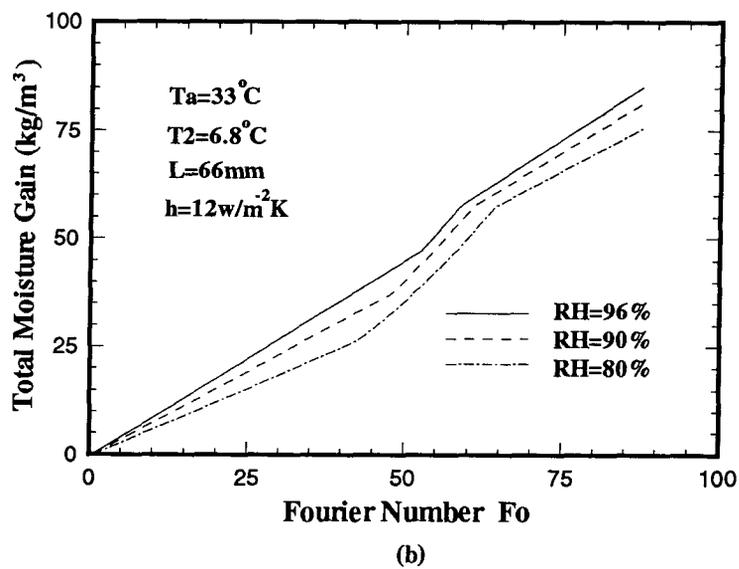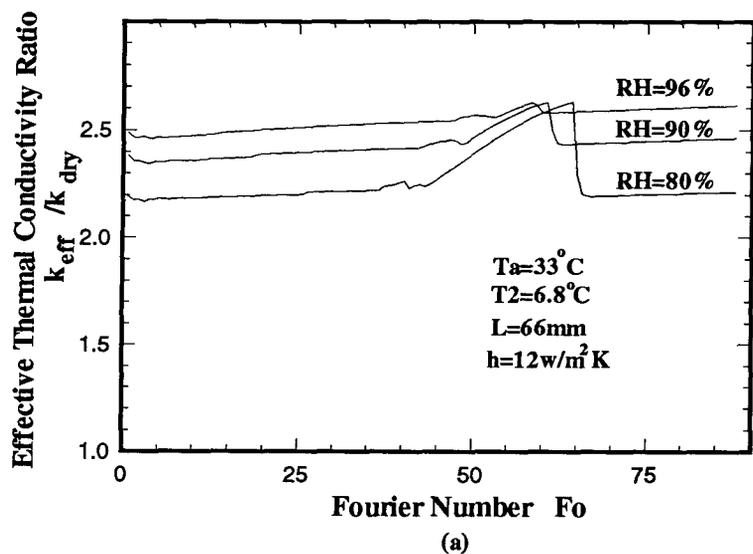
Figure 7.16: The Variation of k_{eff}/k_{dry} at Cold Boundary and Total Liquid Concentration under Different Humidity Levels; $\rho^* = 53$ kg/m^3.

(a)

(b)
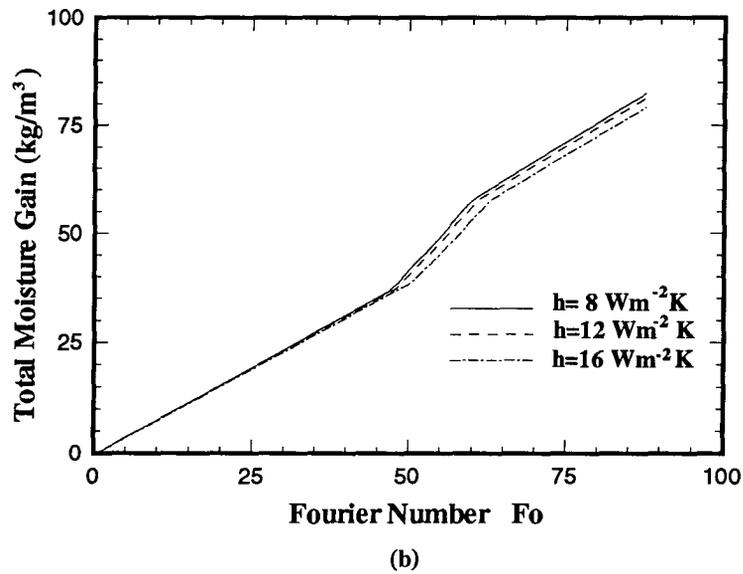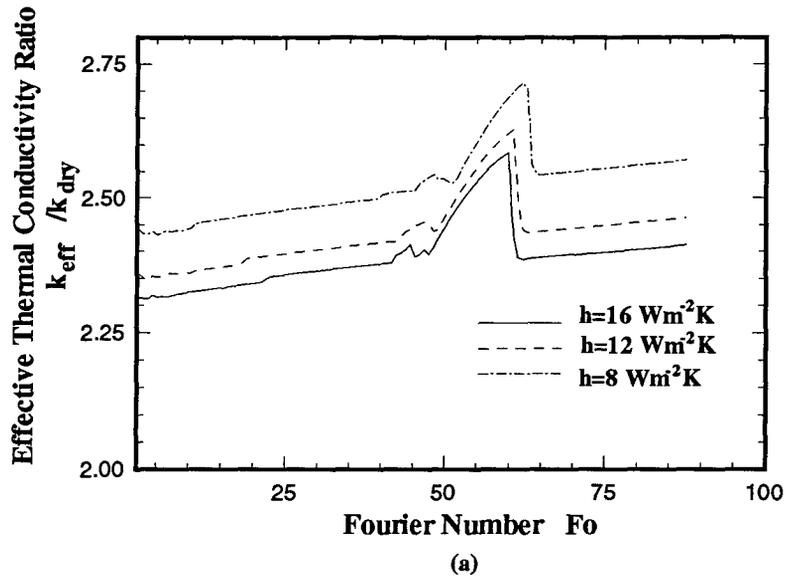
Figure 7.17: The Variation of k_{eff}/k_{dry} at Cold Plate and Total Liquid Concentration under Different Convective Heat Transfer Boundary Conditions; $\rho^* = 53$ kg/m^3, $T_a = 33^\circ C$, $T_2 = 6.8^\circ C$, $L = 66$ mm, $RH = 90\%$.

(a)

(b)
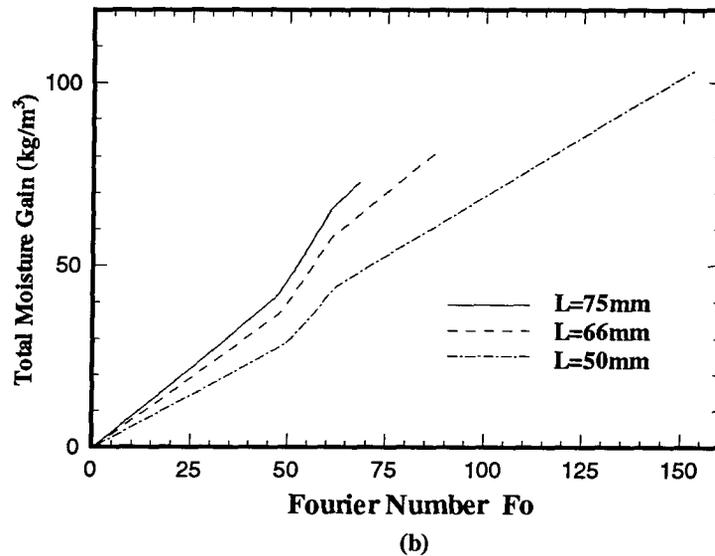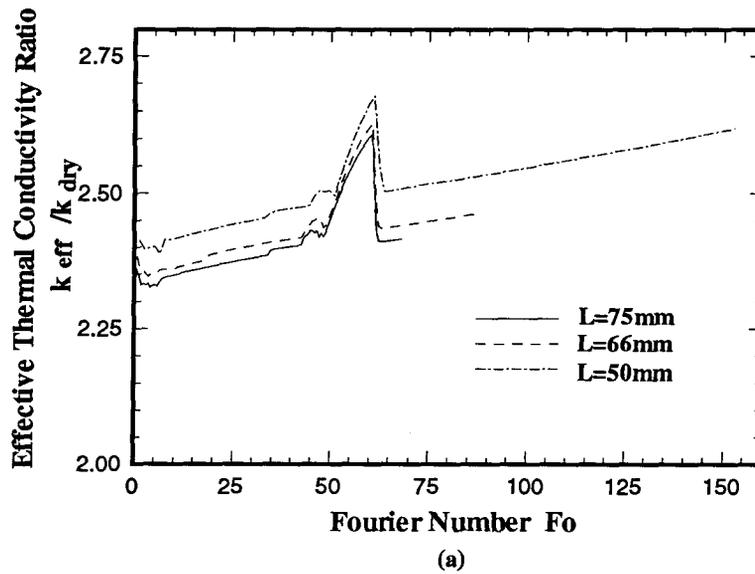
Figure 7.18: The Variation of k_{eff}/k_{dry} at Cold Boundary and Total Liquid Concentration under Different Slab Thickness; $\rho^* = 53$ kg/m^3, $T_a = 33°C$, $T_2 = 6.8°C$, $h^* = 12$ W/m^2 K, $RH = 90\%$.

(a)

(b)
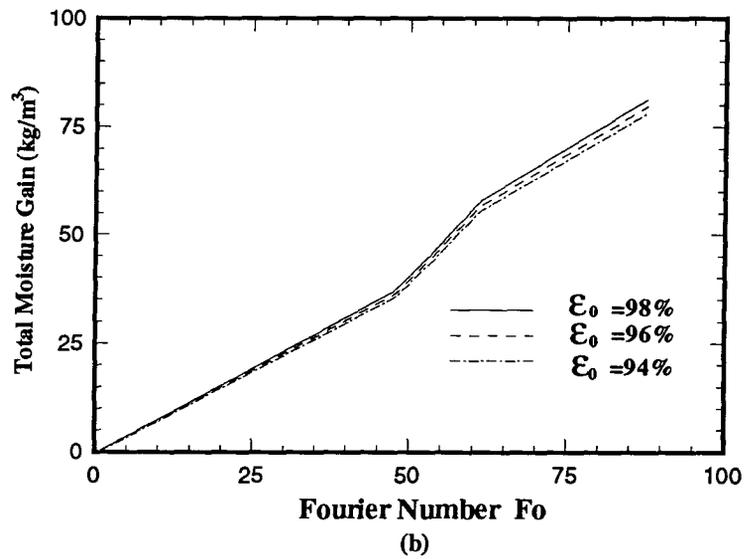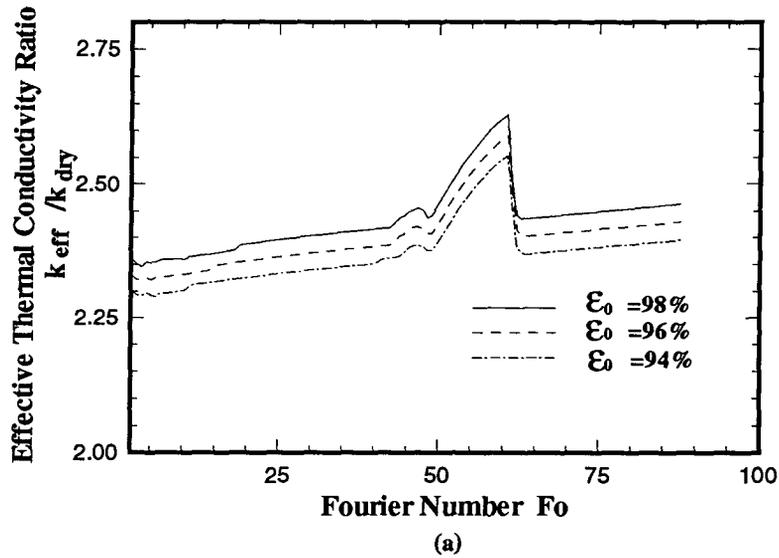
Figure 7.19: The Variation of k_{eff}/k_{dry} at Cold Boundary and Total Liquid Concentration under Different Porousities; $\rho^* = 53$ kg/m^3, $T_a = 33°C$, $T_2 = 6.8°C$, $L = 66$ mm, $h^* = 12$ W/m^2 K, $RH = 90\%$.

thickness, both k_{eff}/k_{dry} and the average liquid concentration increase. This is because temperature diffusion is fast in a thinner slab, and vapor saturation will occur earlier with a thinner slab. Within the same period, the liquid accumulated in a slab increases with decreasing slab thickness; thus the moisture laden conductive heat and latent heat also increase.

7.5.5 Effect of Porosity

Fig. 7.19 shows that the variation in porosity does not have significant effect on the thermal performance and liquid accumulation in a porous insulation. For practical use, the porosities for most of fibrous insulation fall into a narrow range due to their highly porous characteristics. However, examining the effect of porosity can still give us the trend of energy and mass transfer under the influence of porosity. The k_{eff}/k_{dry} and average liquid concentration increase with increasing porosity.

7.5.6 Comparison of Different Thermal Conductivity Models

The apparent thermal conductivity of porous insulation in the presence of liquid is greatly dependent on the liquid distribution in an insulation. Appendix B gives several possible models for k available in literature [2], [43]. These models include bead arrangement, series arrangement, parallel arrangement and form arrangement, based on the manner of liquid location in the pores of insulation.

The variation of k_{eff}/k_{dry} with time using different k models is shown in Fig. 7.20. The parallel arrangement model gives maximum rates of heat transfer. The bead arrangement model gives better trend-wise agreement with the measured heat flux at cold plate for all runs; it is recommended for computational use. The actual distribution of liquid in the insulation is not completely known. However, the above models give an indication of the sensitivity of the predicted quantities to the variation in these important
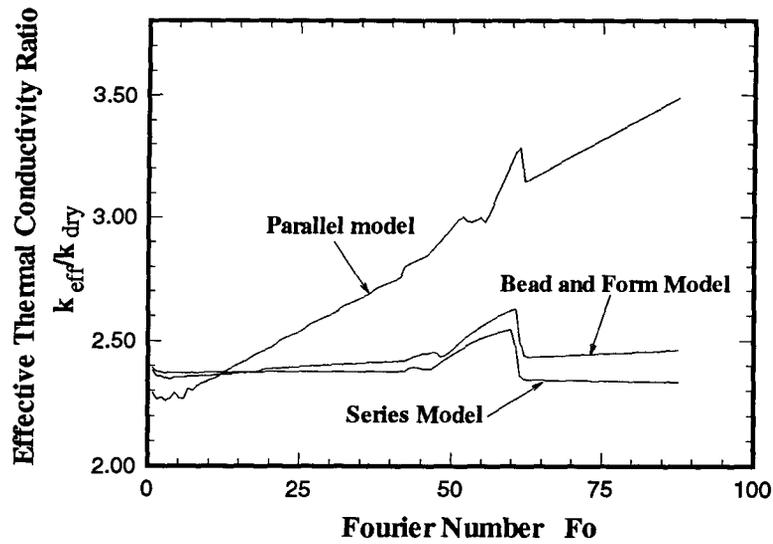
Figure 7.20: The Variation of k_{eff}/k_{dry} at Cold Surface Using Different k Models; $\rho^* = 53$ kg/m^3, $T_a = 33^\circ C$, $T_2 = 6.8^\circ C$, $L = 66$ mm, $h^* = 12$W/m^2 K, $RH = 90\%$.

physical properties.

Chapter 8

CONCLUSIONS AND RECOMMENDATIONS

The following conclusions can be drawn from the analytical and numerical studies on heat and moisture transfer through a porous insulation given in the previous chapters.

8.1 Analytical Study

- The analytical model developed for the heat and water vapor transfer through flat-slab and round pipe insulation is valid for describing the problem of condensation in porous insulation due to thermal and vapor diffusion.

- The effective thermal conductivity and other heat transfer parameters are strongly affected by condensation. The effective thermal conductivity is a maximum when condensation first occurs in the slab. For practical operating conditions its magnitude varies from about 1.5 to 15 times the dry-state value.

- The effective thermal conductivity and other heat transfer parameters depend on seven independent design and operating variables. A parametric study shows that the effective thermal conductivity increases with the increasing ambient humidity level and porosity, and decrease with increasing ambient heat transfer coefficient, slab thickness and dry-state thermal conductivity of insulation.

- The design curves are presented for flat-slabs. They may be used for round-pipe insulation by computing the equivalent flat-slab thickness of the insulation.

8.2 Numerical Study

- The analysis in the present work has identified the four stages of heat and moisture transfer in a porous insulation. A wave-like propagation phenomenon has been observed for the important field variables such as the temperature and vapor density in the initial stage. The dynamic response and transient behavior with condensation and liquid diffusion processes are clearly shown. The numerical prediction of quasi-steady behavior has verified the analytical results, and the long term behavior of energy and moisture transfer through a porous insulation has been presented.

- The numerical model simulates the heat and moisture transport process through a porous insulation successfully. The predicted temperature distributions, heat transfer rates and total moisture gains have good agreements with the experimental results over various operating conditions for a time period up to 600 hours.

- The present model gives reasonable prediction of liquid distribution for the situations in which liquid concentration in an insulation is low. For a complete interpretation of liquid distribution, a more accurate liquid diffusion coefficient model based on experimental work is required.

- The effects of important parameters on heat and mass transfer have been investigated. The heat transfer is strongly affected by moisture distribution. The transient effective thermal conductivity increases with increasing exterior humidity level and porosity, and also increases with decreasing convective heat transfer coefficient and slab thickness.

8.3 Recommendations

It is clear from previous comparisons and discussions that a complete simulation of heat and moisture transfer through a porous insulation will require more rigorous theoretical work, as well as more thorough and accurate experimental work. The following recommendations are suggested for a future work.

- Due to lack of information on liquid diffusivity and hydraulic conductivity of fibrous insulations, more accurate experimental work on physical properties and transport performance of fibrous insulation is greatly needed.

- A two-dimensional numerical model is needed in order to interpret a tendency of liquid movement along the fibers. This may be important for the cases where the pressure gradient in an insulation is low.

- The present numerical model can be improved by removing some simplifications. The effects of air infiltration, gravitation, and varied pressure in an insulation would be taken into account for practical applications.

- It would be interesting to extend the subject of the present study to a similar problem with two permeable boundaries which represents the common situation in building envelopes.

Bibliography

[1] Lotz, W. A., "Moisture problems in buildings in hot humid climates", ASHRAE J., April 1989.

[2] Kaviany, M., "Principles of heat transfer in porous media", Springer-Verlag, New York, 1991.

[3] Whitaker, S., "Simultaneous heat, mass and momentum transfer in porous mediua: A theory of drying", Advance in Heat Transfer, Vol. 13, 119-203, 1977.

[4] Krischer, O., " The heat, moisture, and vapor movement during drying porous materials", VDIZ., Beih. 1, 17-24, 1990.

[5] Philip, J.R., and De Vries, D.A, "Moisture movement in porous materials under temperature gradients", Trans. Am. Geo. Union, 38:222-232, 1957.

[6] De Vries, D.A., "Simultaneous transfer of heat and moisture in porous media", Trans. Am. Geo. Union, 39: 909-916, 1958.

[7] Luikov, A.V., "Heat and mass transfer in capillary-porous bodies", Pergamon, Oxford, 1966.

[8] Luikov, A.V., "System of differential equations of heat and mass transfer in capillary porous bodies (review)", Int. J. Heat Mass Transfer 18: 1-14, 1975.

[9] Cary, J.W., and Taylor, S.A., "The interaction of the simultaneous diffusion of heat and water vapor", Soil Sci. Soc. Am. Proc. 26:413:416, 1962.

[10] Huang., C.L.D., "Multi-phase moisture transfer in porous media subjected to temperature gradient", Int. J. Heat Mass Transfer, 22:1295-1307, 1979.

[11] Eckert, E.R.G., and Faghri, M., "A general analysis of moisture migration caused by temperature differences in an unsaturated porous medium", Int. J. Heat Mass Transfer, 23: 1613-1623, 1980.

[12] Jespersen, H.B., "Thermal conductivity of moisture materials and its measurements", J. Inst. Heat Vent. Engrs 1, pp. 216-222, 1953.

[13] Joy, F.A., "Symposium on thermal conductivity measurements and applications of thermal insulations", ASTM STP 217 65-80, 1957.

[14] Langlais, C., Hyrien,M., and Klarsfeld,S., "Moisture migration in buildings", ASTM STP 779 192-206, 1982.

[15] Bomberg, M. and Shirtliffe, C. J., "Influence of moisture gradients on heat transfer through porous building materials, thermal transmission measurement of insulation", ASTM STP 660, R.P. Tye, ed., American Society for Testing and Materials, 211-233, 1978.

[16] Kumaran, M. K., " Moisture transport through glass-fibre insulation in the presence of a thermal gradient", J. of Thermal Insulation, 10:243-255, 1987.

[17] Kumaran, M. K., "Comparison of simultaneous heat and moisture transport through glass-fiber and spray-cellulose insulations", J. of Thermal Insulation, 12 :6-16, 1988.

[18] Langlais, L. C., Hydrien, M. and Klarsfeld, S., " Influence of moisture on heat transfer through fibrous insulating materials, thermal insulation, materials and systems for energy conservation in the 80's." ASTM STP 789, Govan, F. A., Greason, D. M. and McAllister, J. D., eds., American Society for testing and materials, 563-581,1983.

[19] Langlais, C. and Klarsfeld, S., " Heat and mass transfer in fibrous insulation", J. Thermal Insulation, 8:49-80, 1984.

[20] Thomas, W. C., Bal, G. P. and Onega, R. J., " Heat and mass transfer in glass fibre roof insulating materials", ASTM STP American Society for Testing and Materials, pp. 582-601, 1984.

[21] Modi, D. K., and Benner, S. M., " Moisture gain of spray applied insulations and its effect on effective thermal conductivity - Part I", J. of Thermal Insulation, 8:259-277, 1985.

[22] Benner, S. M. and Modi, D. K., "Moisture gain of spray applied insulations and its effect on effective thermal conductivity - Part II", J. of Thermal Insulation, 9:211-223, 1986.

[23] Wijeysundera, N. E., Hawlader, M. N. A. and Tan, Y. T., "Water vapour diffusion and condensation in fibrous insulations", Int. J. Heat Mass Transfer, 32(10): 1865-1878, 1989.

[24] Wijeysundera, N. E., Hawlader, M. N. A. and Lian, S. C., " An experimental study of condensation in fiberglass insulations", Paper FE89-32 ASHRAE Far East Conference on Air Condition in Hot Climates, Kuala Lumpur, Malaysia, October 25-28, 1989.

[25] Wijeysundera, N.E., and Hawlader, M.N.A., "Effect of condensation and liquid transport on the thermal performance of fibrous insulations", Int. J. Heat Mass Transfer, 35: 2605-2616, 1992.

[26] Motakef, S. and El-Masri, M. A., " Liquid diffusion in fibrous insulation", ASME, J. Heat Transfer, 107:229-306, 1985.

[27] Timusk, J., and Tenender, L.M., "Mechanism of drainage and capillary rise in glass fibre insulation", J. Thermal Insulation, 11: 231-241, 1988.

[28] Cid, J., and Crausse, P., "Influence of the structural characteristic of fibrous heat insulators upon their properties of moisture transfer", J. Thermal Insulation, 14: 123-134, 1990.

[29] Hedlin, C. P., "Heat transfer in a wet porous thermal insulation in a flat roof", J. of Thermal Insulation, 11:165-188, 1988.

[30] Dinulescu, H.A., and Eckert, E.R.G., "Analysis of the one-dimensional moisture migration caused by temperature gradients in porous medium", Int. J. Heat Mass Transfer, 23: 1069-1078, 1980.

[31] Ogniewiez, Y. and Tien, C. L., "Analysis of consensation in porous insulation" , Int. J. Heat Mass Transfer, 24:421-429, 1981.

[32] Motakef, S. and El-Masri, M. A., "Simultaneous heat and mass transfer with phase change in a porous slab", Int. J. Heat Mass transfer, 29(10): 1503- 1512, 1986.

[33] Vafai, K., and Sarkar, S., "Condensation effects in a fibrous insulation slab", ASME J. Heat Transfer, 108:667-675, 1986.

[34] Shapiro, A. P. and Motakef. S., " Unsteady heat and mass transfer with phase change in porous slab: analytical solutions and experimental results", Int. J. Heat Mass Transfer, 33(1): 163-173, 1990.

[35] Vafai, K and Witaker, S., " Simultaneous heat and mass transfer accompanied by phase change in porous insulation", Trans. ASME, J. Heat Transfer, 108:132-140, 1986.

[36] Vafai, K and Tien, H. C., " A numerical investigation of phase change effects in porous materials", Int. J. Heat and Mass Transfer, 23(7): 1261-1277, 1989.

[37] Tien, H.C., and Vafai, K., "A synthesis of infiltration effects on an insulation matrix", Int. J. Heat Mass Transfer, 33:1263-1280, 1990.

[38] Tao, Y. -X., Besant, R. W. and Rezkallah, "Unsteady heat and mass transfer with phase changes in an insulation slab: frosting effects", Int. J. Heat Mass Transfer, 34(7): 1593-1603, 1991.

[39] Edwards D. K., Denny, D. E. and Mills, A. F., "Transfer process: a introduction to diffusion, convection and radiation", New York, McGraw-Hill, 1979.

[40] Woodside, W., "Probe for thermal conductivity measurements of dry and moist materials", Heat pipe. Air Cond. 30, pp. 163-170, 1958.

[41] Crausse, P., Bacon, C. and Langlais C., " Experimental and theoretical study of simultaneous heat and moisture transfer in a fibrous insulation", J. of Thermal Insulation, 9:46-67, 1985.

[42] Patankar, S.V., "Numerical heat transfer and fluid flow", New York, McGraw-Hill, 1980.

[43] Batty, W.J., O'Callaghan P.W. and Probert, S.D, "Apparent thermal conductivity of glass-fiber insulant: effects of compression and moisture content", Applied Energy, 9:55:76, 1981.

[44] Pallady, P.H. and Handley, P.J., "Evaluating moist air properties", Chemical Engineering, 10:, 1984.

[45] Defay, R., Prigogine, I., and Bellemans, A., "Surface tension and adsorption", Wiley, New York, 1966

Appendix A

Water Vapor-Air Mixture Diffusion

A.1 Vapor Diffusion Coefficient in Porous Media

The mass transfer of a water vapor-air mixture within the pores of a porous medium occurs by two mechanisms: ordinary diffusion and Knudsen diffusion [39]. The Knudsen diffusion refers to the case that the pores are small or the gas density is very low, therefore the molecules collide with the pore walls more frequently, and diffusion of molecules along the pore wall is described by the equations for free molecule or Knudsen flow.

Porous insulation usually has a very high porosity. The vapor-air mixture is relatively dense. The vapor diffusion in porous insulation is dominated by ordinary diffusion which can be described by Fick's law.

The vapor-air mixture diffusion coefficient in porous insulation, therefore, can be taken to be [39]:

$$D_v^* = \frac{\epsilon_0}{\tau} D_{12},$$
(A.1)

where D_{12} is the binary diffusion coefficient of Fick's law; ϵ_0 is the porosity; τ is the tortuousity, accounting for the increased diffusion length due to tortuous paths of real pores, and for the effects of constrictions.

Diffusion coefficients of gases at low pressure are almost composition independent, and increase with temperature. According to reference [23], the binary diffusion coefficient for water vapor-air mixture is given by:

$$D_{12} = 1.97(10)^{-5}(\frac{T}{255.2})^{1.685}. \qquad (A.2)$$

A.2 Mass Transfer Coefficient in Ambient

To determine the mass transfer coefficient between the ambient air and the insulation slab, an analysis of a slug flow over a slab surface is conducted. According to reference [39], the solution for the average heat transfer coefficient over a length of the flat surface is:

$$h^* = \frac{2k^*}{\pi^{1/2}}(\frac{V_m}{\alpha^* L})^{1/2}. \qquad (A.3)$$

A similar solution can be derived for the average mass transfer coefficient over a length L:

$$h_m^* = \frac{2\rho_a^* D_{12}^*}{\pi^{1/2}}(\frac{V_m}{D_{12}^* L})^{1/2}, \qquad (A.4)$$

where V_m is the main stream velocity.

Comparing the above two expressions, one could obtain:

$$\frac{h_m^*}{h^*} = \frac{\rho_a^* D_{12}^*}{k}(\frac{\alpha^*}{D_{12}^*})^{1/2}. \qquad (A.5)$$

Note that (α^*/D_v^*) is the Lewis number, which characterizes the ratio of thermal and mass diffusion. For quasi-steady phase, the Lewis number may be assumed to be unity. Wijeysundera et al. [23] gave a modified expression for mass transfer coefficient:

$$h_m^* = (\frac{h^*}{1.047})(\frac{\rho_a^* D_{12}^*}{k^*}). \qquad (A.6)$$

A.3 Calculation of Vapor Concentration in Ambient

The vapor concentration (or vapor density) of the ambient air needs to be calculated. This is done based on the saturated vapor pressure and relative humidity in the section. The equations for the determination of the saturated vapor pressure were obtained by using a mathematical fit of the pyschometric chart by Pallady and Hanley [44].

$$KD = -8.83(10)^{-10}TR^3 + 3.07(10)^{-6}TR^2 - 3.47(10)^{-3}TR + 4.4, \qquad (A.7)$$

$$F = KD(1 - 1165.7/TR) + 5, \qquad (A.8)$$

$$PD = 1.668(10)^F, \qquad (A.9)$$

where, PD is the saturated vapor partial pressure in mm of mercury, and TR is temperature in $^{\circ}R$.

The vapor partial pressure in bar is:

$$p_v^* = RH\frac{PD}{760}. \qquad (A.10)$$

The vapor density in ambient can be obtained from gas state equation:

$$p_v^* = \rho_v^* R_v T. \qquad (A.11)$$

The concentration of vapor is:

$$m_v = \frac{\rho_v^*}{\rho_v^* + \rho_a^*}. \qquad (A.12)$$

The air density can be obtained from gas state equation by assuming the total pressure is 1 atmospheres.

Appendix B

Thermal Conductivity of Moist Insulation

The presence of moisture has a significant effect on apparent thermal conductivity of porous insulation. It is believed that the apparent thermal conductivity of moist insulation depends on the manner that the liquid distributes inside the insulation [43].

Four different physical models for liquid distribution in a porous medium are considered in the present study.

(a) Bead arrangement.

In this model liquid is located as small beads throughout the insulant. The apparent thermal conductivity can be represent by:

$$k^*(\epsilon_\beta) = k_d^* \frac{(1 + \epsilon_\beta Y)}{(1 - \epsilon_\beta Y)},$$ (B.13)

where

$$Y = \frac{(k_\beta^* - k_d^*)}{(k_\beta^* + 2k_d^*)}.$$ (B.14)

(b). Series arrangement.

In this model the liquid is distributed in layers perpendicular to the direction of heat flow. The liquid would then have the maximum effect in inhibiting the heat flow.

For this arrangement,

$$k^*(\epsilon_\beta) = \frac{k_d^* k_\beta^*}{k_\beta^* - X},$$ (B.15)

105

where

$$X = \frac{\epsilon_\beta}{\epsilon_\gamma}(k_\beta^* - k_d^*).$$

(B.16)

(c). Parallel arrangement.

In this model the liquid is located in a continuous shape parallel to the direction of heat flow.

For this arrangement,

$$k^*(\epsilon_\beta) = k_d^* + X,$$

(B.17)

where

$$X = \frac{\epsilon_\beta}{\epsilon_\gamma}(k_\beta^* - k_d^*).$$

(B.18)

(d) Form arrangement.

In this model a liquid film surrounds each insulant fiber or particle; the films thereby forming a honeycomb structure.

The same formula as that for bead arrangement can be used for the form arrangement.